The Attenuating Effects of 14-3-3η in Parkinson's Disease-Related α-Synuclein Aggregation

By Mette Ovesen

Thesis submitted in partial fulfillment of the requirements for the degree of

Master of Science

Department of Biological Sciences

Faculty of Mathematics and Natural Sciences

University of Bergen

June 2020

ACKNOWLEDGEMENTS

TABLE OF CONTENTS

SELECTED ABBREVIATIONS

AD — Alzheimer's Disease

ALS — Amyotrophic lateral sclerosis

APPW — Average percentage of positive wells

BSA — Bovine serum albumin

CJD — Creutzfeldt-Jakob Disease

CL — Cell lysate

CSF — Cerebrospinal fluid

FAs — Fatty acids

HD — Huntington's Disease

HSQC — Heteronuclear single quantum coherence spectroscopy

LB medium — Lysogeny broth medium

LBs — Lewy bodies

NAC — Non-amyloid β-component

NDs — Neurodegenerative diseases

NFPs — Non-fibrillar products

NMR — Nuclear magnetic resonance

PAGE — Polyacrylamide gel electrophoresis

PC — Periplasmic content

PD — Parkinson's Disease

PN — Proteostasis network

PTMs — Post-translational modifications

RU — Response units

SDS — Sodium dodecyl sulfate

SEC — Size exclusion chromatography

SPR — Surface plasmon resonance

ThT — Thioflavin T

TROSY — Transverse relaxation-optimized spectroscopy

αS — α-Synuclein

ABSTRACT

Characterized by the progressive loss of dopaminergic neurons, Parkinson's Disease (PD) is one of the most common neurodegenerative diseases (NDs). A pathological hallmark of PD is the presence of neuronal inclusions termed Lewy Bodies (LBs). The main component of LBs has been identified as α-Synuclein (αS): a small synaptic protein with an intrinsically disordered structure in its native state. In parkinsonian brains, αS abnormally aggregates into fibrillar β-sheet rich structures that accumulate in LBs. Consequently, the misfolding and aggregation of αS has been established as central in PD pathology.

In recent years, several studies in neuroprotection have focused on 14-3-3 proteins – a family of adaptor proteins with chaperone activities, consisting of seven human isoforms. With regards to PD, several 14-3-3 isoforms have been detected in LBs and shown to interact with PD related proteins like αS and Parkin. In particular, the 14-3-3η isoform has been found to co-immunoprecipitate with αS in parkinsonian brains. Previous aggregation studies have also demonstrated that this isoform interferes with αS aggregation by rerouting the fibrillation process. Moreover, studies in aging mice overexpressing αS demonstrated an upregulation of 14-3-3η, altogether indicating a role of 14-3-3η in αS aggregation and PD in general.

In this study, we investigated how 14-3-3η in different αS:14-3-3 ratios affect the kinetics of αS aggregation *in vitro* by Thioflavin T (ThT) monitored aggregation assays. Our findings show 14-3-3η to decrease αS fibril growth rate by more than 50% in ratios of 10:1 and 2:1. The fibrillation lag time, and thus onset, was not significantly affected by 14-3-3η. However, this could be attributed to an insufficient number of replicates, and we concluded that 14-3-3η likely attenuates αS fibrillation onset as well. We further sought to locate the 14-3-3η residues involved in αS binding by nuclear magnetic resonance (NMR) spectroscopy and to characterize the binding by surface plasmon resonance (SPR) experiments. Although time restrictions prevented binding site analysis, we found that $^2H^{13}C^{15}N$-labeling and TROSY-HSQC experiments considerably improves the 14-3-3η fingerprint spectrum, enabling future binding analysis. SPR experiments indicated no binding of 14-3-3η to monomeric αS, suggesting that the binding occurs at oligomeric stages of αS aggregation. In sum, we propose that 14-3-3η interacts with αS oligomers to attenuate αS fibril growth, and possibly fibrillation onset.

1. INTRODUCTION

Neurodegenerative diseases (NDs) are a diverse group of diseases involving the progressive damage or death of neuronal cells. Different parts of the brain or central nervous system can be affected, resulting in clinical symptoms such as cognitive decline, motor deficiencies, dementia and ataxia (incoordination, speech impediments)[1]. Despite their growing incidence, efforts to find treatments have yielded little success, and no effective therapies currently exist. While the most common NDs are Alzheimer's disease (AD) and Parkinson's disease (PD), they also include disorders such as Huntington's disease (HD), Amyotrophic Lateral Sclerosis (ALS) and Creutzfeldt-Jakob Disease (CJD)[1,2]. Although NDs present with diverse symptoms and distinct disease progressions, there are certain similarities; (i) they all present in later stages of life, making age a large risk factor, (ii) with a few exceptions, each disease has a sporadic and a familial variant, and (iii) their pathology can be characterized by synaptic abnormalities and neuronal loss[1]. Another important hallmark of many NDs is the phenomenon of protein aggregation, which leads to abnormal cellular protein deposits. Hence, a better understanding of the pathways involved in protein aggregation, accumulation and toxicity mechanisms is viewed as a promising path to finding therapeutic targets[3].

1.1 PROTEIN MISFOLDING AND DISEASE

Several NDs are referred to as proteinopathies, characterized by disease-specific proteins that misfold and aggregate into larger insoluble structures[2]. Although the misfolded aggregates are generally inactive, their accumulation can trigger cellular stress responses and inflict proteotoxic damage to the cells in question[4]. Post-mitotic neurons are especially vulnerable to this problem[4]. Despite the different mechanisms and pathways through which proteins may aggregate, the final structures are usually fibrous and comprised of misfolded proteins in β-sheet conformations. Termed amyloids, these aggregates or inclusions are deposited in neurons of specific brain regions, ultimately leading to neuronal apoptosis and neurodegeneration[3]. However, the mechanisms mediating neurotoxicity remain enigmatic in the question of ND-related protein aggregation. Whether the protein aggregates are directly involved in the pathogenesis has not yet been determined with certainty. It has been suggested that amyloid deposits represent an endpoint of a molecular cascade where the earlier stages are more directly linked to the pathogenesis than the final aggregates[1,3]. Nevertheless, specific aggregating proteins have been identified as central players in different proteinopathies (Figure 1.1).

Examples include deposits of Tau and Amyloid β found in AD, mutations and accumulation of Huntingtin in HD, and fibrillar α-Synuclein (αS) present in neuronal inclusions of PD brains[5].
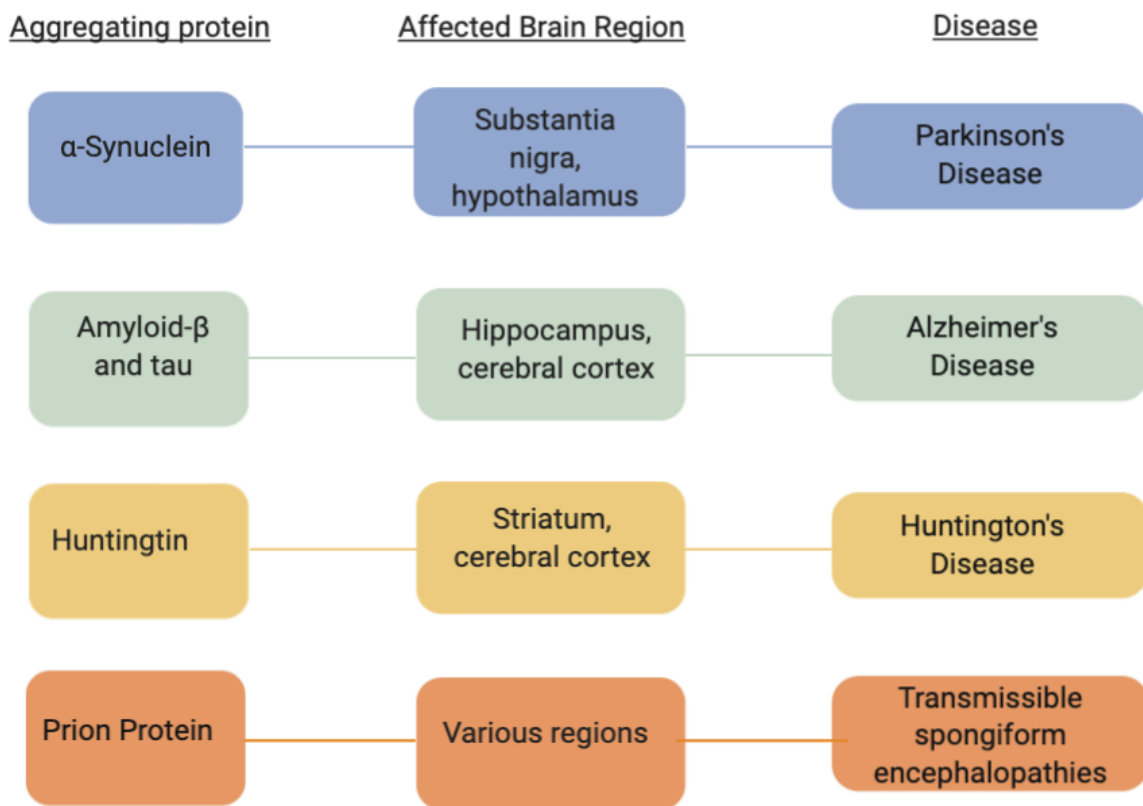
Figure 1.1 – Disease-specific proteins and the affected brain regions in neurodegenerative diseases. Protein aggregation has become a hallmark of many neurodegenerative diseases. Disease-specific proteins like α-Synuclein, Amyloid β, Huntingtin and Prion proteins are all connected to a neurodegenerative disease through their aggregation and effects on the brain[1]. Figure created in BioRender.com, and adapted from Soto *et al*[1].

1.2 α-SYNUCLEIN AGGREGATION – A HALLMARK OF PARKINSON'S DISEASE

PD is the second most common ND in the world today[6], affecting an estimated 2% of the population above 60 years of age[7]. As there is currently no cure nor efficient means of early diagnosis, the underlying pathogenesis of PD has become an important field of research[7,8]. Characterized by the progressive loss of dopaminergic neurons in the substantia nigra pars compacta[9], PD leads to clinical symptoms such as resting tremors, rigidity and bradykinesia, as well as non-motor symptoms like depression, cognitive decline and eventually mood alterations and dementia[7]. Although no definitive cause of PD has been determined, a hallmark of PD is the presence of insoluble inclusions called Lewy Bodies (LBs) in the affected neurons[8,9]. LBs are mainly composed of fibrillar aggregates of αS, a small protein normally found at the pre-

synaptic terminals[10]. In addition to αS accumulating in the LBs found in sporadic PD, point mutations or gene duplication of αS can also produce a dominant inherited form of the disease: familial PD[8,10,11]. Furthermore, overexpression of wild-type αS in cell-culture systems and animal models has led to neurodegeneration in dopaminergic neurons[11], altogether pointing to a central and possibly causative role of αS in the pathogenesis of PD.

1.3 THE STRUCTURE AND FUNCTION OF α-SYNUCLEIN

Comprised of 140 amino acid residues, αS is a small acidic protein abundantly expressed in the human brain and predominantly found in the pre-synaptic terminals[12]. In its soluble cytosolic form, αS is termed an intrinsically disordered protein due to its lack of stable secondary and tertiary structures[12]. αS can be divided into three biochemically and functionally distinct regions (Figure 1.2): (i) an amphipathic N-terminal region, (ii) a hydrophobic non-amyloid β-component (NAC) and (iii) an acidic C-terminal[13]. Whereas the majority of post-translational modifications (PTMs) or truncations occur on its C-terminal region[13], the N-terminal region is the main site for all known clinical mutations (e.g. A53T, A30P, E46K) that result in familial PD, implying its significance in the misfolding and aggregation of αS[6]. Furthermore, the N-terminal is also where the protein interacts with phospholipid membranes and micelles[13]. The NAC region is also deemed important in the self-aggregation of αS; a stretch of 12 residues in this domain inhibits degradation upon misfolding, and instead promotes the protein's fibrillation[6].
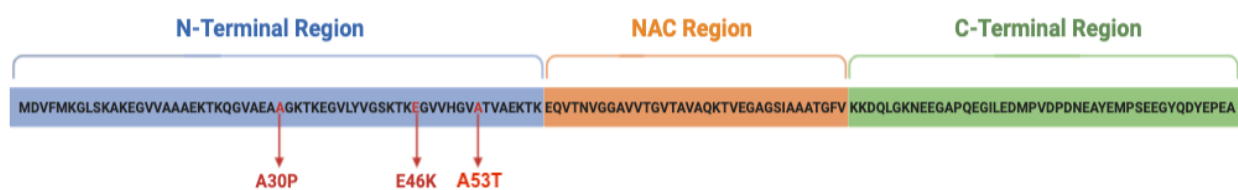
Figure 1.2 – The protein sequence and different regions of the intrinsically disordered α-Synuclein (αS). This small, acidic protein can be divided into three distinct regions; the N-terminal region (blue), the Non-Amyloid Component (NAC) region (orange) and the acidic C-terminal region (green)[13]. Known clinical mutations involved in PD have all been found to occur in the N-terminal region, such as A30P, E46K and A53T (red), while the NAC region is highly involved in the self-aggregation of αS[6]. Figure created in BioRender.com, and adapted from Miraglia *et al*[13].

Hitherto, no exact native function of αS has been uncovered. However, it is not considered an essential protein. Knockout studies in mice demonstrated that αS deficiency did not obstruct their basic brain functions nor affect their survival[14]. Nevertheless, αS localization and interactions with membranes suggest its involvement in regulation of synaptic plasticity, neurotransmitter release, dopamine metabolism and vesicle trafficking[15]. Interestingly, αS interacting with membranes is not only thought to be important for its function. The interaction also produces a conformational change in the protein itself. Upon membrane binding, αS can transition from its disordered state into a helical conformation[12]. Depending on the membrane lipid constitution, membrane-bound αS can adopt one of two proposed structural models: (i) the "extended helix", comprising one single ~100-residue α-Helix, and (ii) the "horse-shoe", made up of two separate helices with different lipid affinities[16]. As such, αS exists in healthy cells either as cytosolic and disordered or helical and membrane-bound.

1.4 FROM DISORDERED MONOMERS TO HIGHLY ORDERED FIBRILS

In contrast to the unfolded state of native αS, the proteinaceous aggregates found in LBs are highly ordered. The αS amyloid fibrils are filamentous in structure and comprised of parallel β-sheets, with a cross-β diffraction pattern and a hydrophobic core – characteristics shared with fibrillar accumulations found in several other NDs[17,18]. Because amyloid fibril formation is a common occurrence *in vitro*, it has enabled extensive research on the general fibrillation process[17]. As such, αS fibrillation is now thought to occur through a nucleation-polymerization model[19]. This model implies that soluble monomeric αS form oligomeric species in a primary nucleation, before these oligomers form protofilaments that will finally constitute the mature fibrils (Figure 1.3)[17].
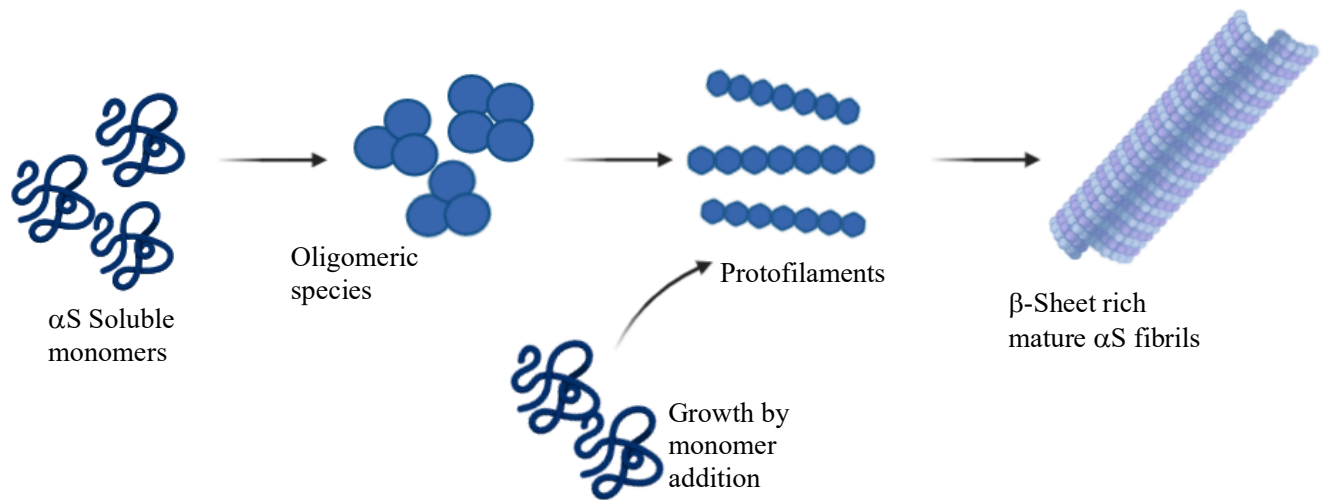
Figure 1.3 – Aggregation of α-Synuclein (αS) occurs through a nucleation-polymerization model to form fibrillar structures. The primary nucleation occurs when misfolding of the intrinsically disordered and soluble αS monomers forms oligomeric species, which are further polymerized to short protofilaments with a high β-sheet content. Subsequent fibril elongation then occurs through a secondary nucleation; incorporation of new monomers enables fibril growth and finally produces the mature insoluble fibrils[17]. Figure created in BioRender.com.

Fibril growth is enabled by the addition of soluble monomers rather than oligomers, in a process termed secondary nucleation[17,20]. The result is a sigmoidal growth profile with three characteristic phases (Figure 1.4). During the lag phase, monomers oligomerize to form the larger oligomeric species. This is followed by the growth phase, when protofilaments and fibrils are constructed from oligomers and elongated by monomers. Finally, the plateau phase is reached, upon which fibril growth is haltered as monomers become depleted[17]. Additionally, preformed fibrils, termed seeds, can enhance αS aggregation *in vivo* in a process termed seeding. Studies of wild-type mice showed that injection of exogenous fibril seeds induced the aggregation of their endogenous αS, leading to a pathology resembling the neurodegenerative pattern of PD[21]. If seeds are present, the lag phase can be drastically reduced, and can accelerate the growth phase and the overall conversion from soluble to aggregated protein, either through elongation or surface-catalyzed secondary nucleation[20]. Although the amyloid fibril assembly has been widely characterized, knowledge of the early oligomerization steps is still limited[17]. Understanding these mechanisms is of great importance – the mechanisms of early oligomerization are not only crucial to αS self-association, but oligomeric species have recently been suggested as the cell toxic factors in PD neurodegeneration[22,23].
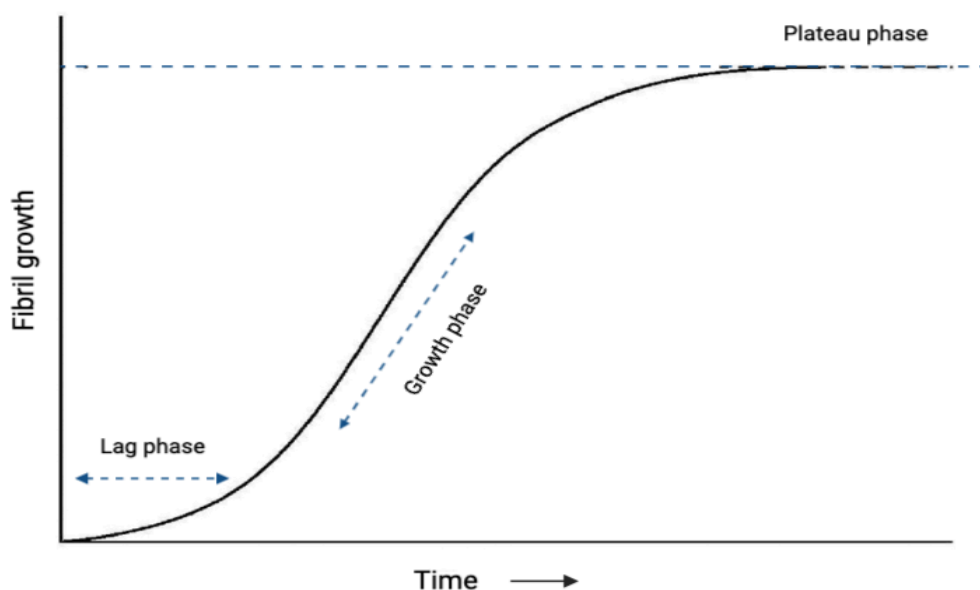
Figure 1.4 – Fibrillation of α-Synuclein (αS) follows a characteristic sigmoidal growth profile. The kinetics of αS aggregation can be divided into three distinct phases: (i) oligomerization of misfolded αS monomers into the first oligomeric nuclei gives rise to the lag phase, (ii) the growth phase where protofilaments are formed and fibril growth occurs through incorporation of monomers, and (iii) the plateau phase, characterized by the stagnation of fibril growth as monomers are depleted[17]. Figure created in BioRender.com.

1.5 SEVERAL FACTORS INFLUENCE α-SYNUCLEIN AGGREGATION

In general, multiple factors can influence protein aggregation – temperature, solution conditions, protein concentrations and chemical modifications can all affect the pathways and kinetics of an aggregating protein[24]. With regards to αS, more specific events can also modulate the self-association of this intrinsically disordered protein.

1.5.1 Lipid association affects α-Synuclein aggregation

As previously mentioned, interaction with lipid membranes causes a conformational change in αS, so it is clear that lipids influence the structure of the protein. However, experiments with monomeric αS and lipid vesicles or membranes also indicate that interaction with membranes could substantially enhance αS aggregation, a phenomenon referred to as membrane-induced aggregation[25]. In conditions with low lipid:αS ratios, the primary nucleation becomes greatly enhanced by αS-lipid interaction. This could be attributed to a high local concentration of αS bound to the lipid surface, where monomers are added from solution, or to a conformational change that may favor nucleation[26]. Conversely, it has been suggested that lipid binding could inhibit nucleation and further aggregation in conditions where lipid:αS ratios are high. The

strong association with a lipid bilayer then stabilizes the helical αS conformation and reduces the amount of αS monomers available for nucleation[27]. Furthermore, the length of fatty acyl chains in the membrane-constituting lipids affects the membrane-binding and aggregation propensity of αS. Indeed, lipids with short, saturated fatty acyl chains have been implied to be a strong contributor to membrane-induced αS aggregation[28].

1.5.2 Post-translational modifications of α-Synuclein

Today, an increasing body of evidence suggests that PTMs of αS could play a key role in the oligomerization and fibrillation of αS as well as LB formation in PD. Phosphorylation in particular has received special attention, as the most prominent modification associated with αS aggregation is its phosphorylation at S129. αS containing this modification has been identified as the primary component of LBs found in PD brains[29], suggesting that it could stimulate abnormal αS aggregation. Furthermore, PPA2, a phosphatase that dephosphorylates S129, has been demonstrated to attenuate the formation of αS aggregates in aging mice brains[30]. However, some PTMs appear to mediate opposite effects; sumoylation of αS is suggested to have a neuroprotective role in PD[29]. Indeed, the sumoylation of αS *in vitro* led to a reversal of its accumulation and fibrillation, while inhibiting sumoylation caused αS inclusions and neurotoxicity in mouse models[31].

1.5.3 The role of the proteostasis network

The general folding process is not without error. Considering that any polypeptide could theoretically adopt a gargantuan number of possible conformations, mistakes are bound to occur even under normal cellular conditions[32]. For this reason, a complex network of molecular chaperone proteins acts to control initial folding processes, conformation maintenance and the degradation of improperly folded and potentially harmful proteins. Referred to as the proteostasis network (PN), it consists of proteins termed molecular chaperones, which through their actions maintain protein homeostasis (proteostasis) in the cell[32,33]. Given that incorrect folding, aggregation and failed degradation of aggregates are characteristics of several NDs, chaperones of the PN have been suggested as modulators of pathogenic pathways in PD[33]. Indeed, molecular chaperones like heat-shock protein 70 and DJ-1 have been shown to interfere with or inhibit the αS aggregation process both *in vitro* and in cellular models[34,35]. As a result of these discoveries and the general importance of the PN, several chaperones are now being explored as potential modulators of αS aggregation and pathogenic PD pathways. Amongst

these proteins are the chaperone-like 14-3-3 family of scaffold proteins, which possess important roles in a great number of cellular processes[36].

1.6 THE UBIQUITOUS 14-3-3 PROTEINS

Expressed in all eukaryotic organisms, 14-3-3 proteins are a highly conserved family of molecular scaffold and adaptor proteins involved in mediating signal transduction[36]. Through their interactions with a wide range of protein partners, these phospho-serine/threonine binding proteins take part in cellular processes such as cell proliferation, growth and apoptosis and intracellular protein trafficking[37]. Because of their important cellular roles, evidence implies dysfunctional regulation of 14-3-3 proteins as a contributor to many human diseases like cancer and NDs[38].

1.6.1 Structural Aspects

The 14-3-3 family consists of several isoforms of ~30 kDa proteins. While the number of isoforms differs between species, they all share high sequence homology and a conserved structure[38]. With regards to the human proteins there are seven different isoforms (β, ϵ, η, γ, θ, ζ and σ), which have all been revealed to exist as homo- or heterodimers with a clamp-like structure (Figure 1.5)[39,40]. Each monomer comprises nine α-helices in an antiparallel arrangement, where the N-terminal regions associate to form a dimer interface mainly driven by hydrophobic and electrostatic interactions[38,39]. The monomers contain charged residues Lys, Arg and Tyr in helices $\alpha 3$ and $\alpha 5$, as well as hydrophobic Val and Ile/Leu residues in helices $\alpha 7$ and $\alpha 9$[41]. Together, these residues form the amphipathic groove in which ligand binding occurs (Figure 1.5)[42]. Furthermore, the positioning of these grooves in the dimer allows for simultaneous binding of two peptides, whether they are in the same protein or two different target proteins[41]. However, only phosphorylated proteins containing specific phospho-serine motifs can bind to this groove. 14-3-3 proteins have been shown to specifically recognize three consensus phospho-peptide sequences: motif I (RSXpSXP), motif II (RX(Y/F)XpSXP) and motif III (pSX_{1-2}–COOH)[36,43], where pS represent phosphorylated Ser (or Thr) residues, and X can be any residue.

Phosphoserine peptides
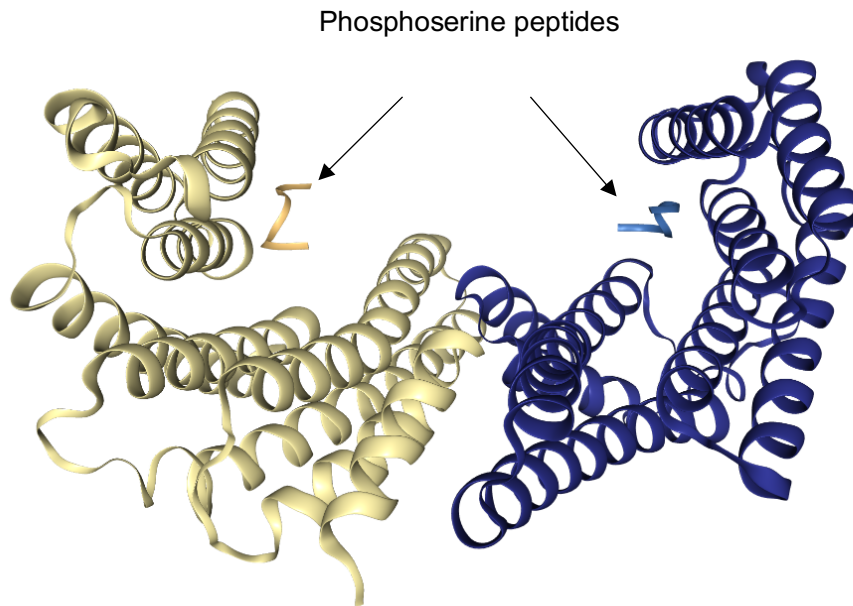
Figure 1.5 – General structure of 14-3-3 protein bound to a phospho-peptide through its canonical binding mode. Proteins in the 14-3-3 family generally exist as homo-or hetero dimers, comprised of ~30 kDa monomers in a clamp-like structure[39]. Charged and hydrophobic residues within helices α3,5,7 and 9 form one amphipathic binding groove for each monomer, positioned to allow for binding of two phospho-peptides or one ligand with two phosphorylation sites[41]. Displayed in the figure is the crystal structure of 14-3-3γ in complex with phosphoserine peptides. Retrieved from *RCSB PDB: 2B05*.

1.6.2 Binding partners and cellular functions

Because the motifs mentioned in Section 1.6.1 are present in a variety of proteins, 14-3-3 proteins associate with a wide range of targets such as kinases and phosphatases, transmembrane receptors, transcription factors and other signaling molecules[38]. Indeed, more than 700 phosphoproteins are identified as possible targets of the 14-3-3 family in humans. Examples include Raf, BAD and Cdc25, which are all important signaling proteins bound by and regulated by different 14-3-3 isoforms[40,41]. The functions of 14-3-3s are thought to be carried out through one of three modes of action: (i) inducing a conformational change in the target protein, stabilizing its structure or accommodating it into the binding groove, (ii) interfering with protein-protein interactions by binding and preventing specific target protein regions from other interactions, or (iii) facilitate interaction between two target proteins by bringing them in close proximity, thus acting as an adaptor protein (Figure 1.6)[38]. Interestingly, some proteins display an isoform-specific affinity towards 14-3-3 proteins. The specific dimer compositions could thus influence which 14-3-3 target proteins that will interact[37].
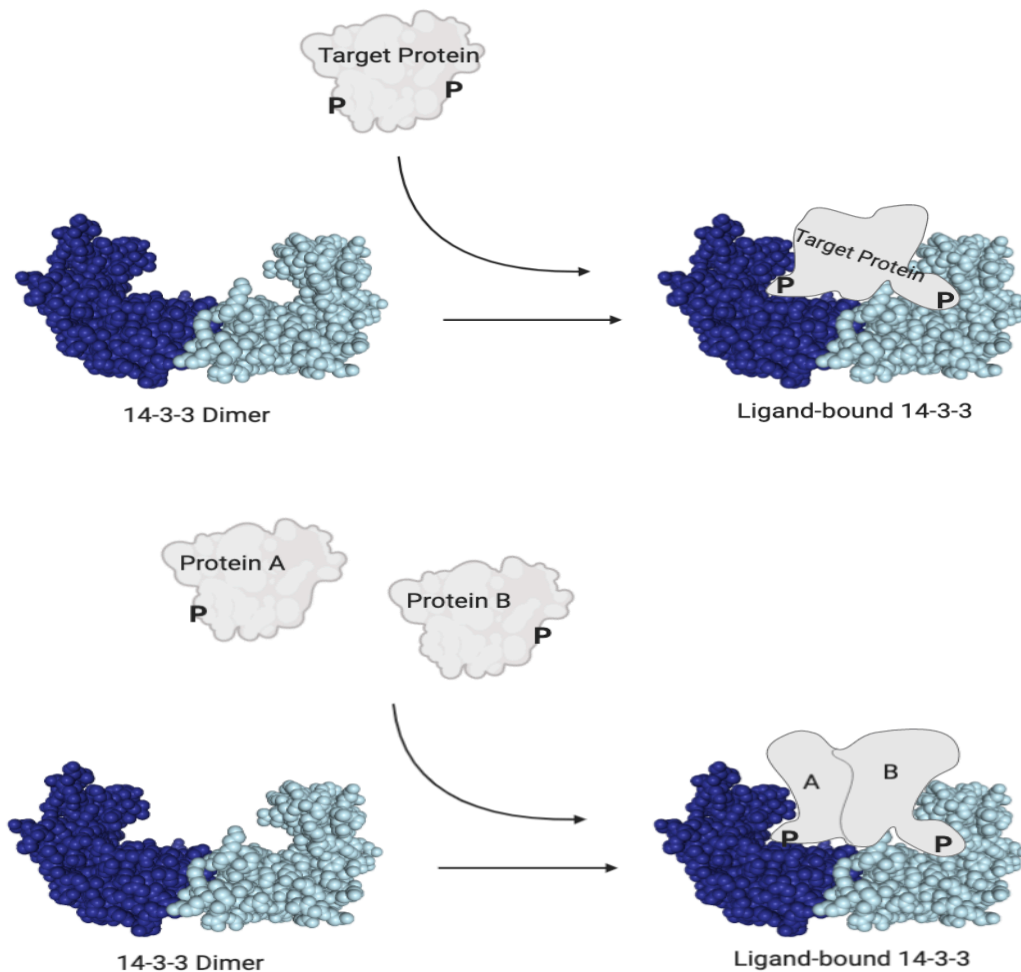
Figure 1.6 – Ligand binding and adaptor function of proteins in the 14-3-3 family. The dimeric structure of 14-3-3 proteins allows simultaneous binding of two phospho-serine motifs, by accommodation into the binding grooves[41]. Through this canonical binding mode, 14-3-3 proteins perform a variety of regulatory functions in the cell. This occurs through the binding of a single protein (top panel) to induce a conformational change, stabilize its structure or shielding it from specific protein-protein interactions, or by bringing two proteins in close proximity (bottom panel) in order to facilitate their interactions[38]. Figure created in BioRender.com, and adapted from Cau *et al*[38].

In addition to their regulatory functions as adaptor/scaffold proteins, 14-3-3 proteins possess a molecular chaperone activity in protein quality control, preventing misfolding or unfolding proteins from aggregating[44]. Upon certain cellular stress conditions, 14-3-3 proteins can interact with unfolded or misfolded proteins to prevent their aggregation or assist in their proteolytic degradation[41]. If this should fail, 14-3-3 proteins have also been shown to mediate the formation of aggresomes, where protein aggregates are deposited to mitigate their toxicity and facilitate macroautophagic removal[39]. However, their chaperone activities are poorly understood, as they seem to be independent of substrate phosphorylation, thus occurring through mechanisms distinct from their canonical phospho-peptide binding mode[41]. Furthermore, several studies

suggest that monomeric forms of 14-3-3 display a more efficient chaperone activity, possibly due to the exposure of hydrophobic regions normally buried in the dimer interface[44,45]. However, further investigations are required to fully understand these mechanisms. Altogether, their many targets and different functions enable 14-3-3 proteins to be an integral part of a multitude of cellular processes like intracellular signaling, intracellular trafficking, transcription, apoptosis, cell cycle regulation and protein quality control[37].

1.6.3 14-3-3 Proteins in neurodegenerative disease

As a result of the variety of important cellular processes they regulate, the 14-3-3 family has been implicated in several human diseases. They are abundantly expressed in the human brain, where they constitute approximately 1% of the soluble protein content and partake in neuronal differentiation and survival, regulation of ion channels, neuronal transmission and synapse plasticity[38], much like the suggested functions of αS. In light of this and their established chaperone activity, 14-3-3 proteins are found to be involved in several NDs, including AD, CJD and PD[38,46]. Furthermore, isoform-specific 14-3-3 knockout studies in mice have resulted in certain syndrome phenotypes and revealed specific 14-3-3 isoform brain functions[47]. Moreover, 14-3-3 isoforms β, ε, η and γ are found in the cerebrospinal fluid (CSF) of patients with CJD, and 14-3-3η was also found in the CSF from patients with other types of dementia such as AD[48]. Further supporting their involvement in neurodegeneration is the presence of 14-3-3 proteins in LBs and neurofibrillary tangles characteristic of PD and AD brain sections, respectively[47,49]. Importantly, several isoforms are also able to interact with specific proteins involved in the pathogenesis of AD, ALS and PD[47]. With regards to PD, certain isoforms can interact with αS and other PD-related proteins like Parkin, Tyrosine hydroxylase and LRRK2[38]. In particular, the 14-3-3η isoform appears to interact with and affect αS in its aggregation process[9].

1.7 AN ISOFORM OF INTEREST – 14-3-3η

With a size of 28 kDa, 14-3-3η is a 14-3-3 isoform found in the cytosol or the extracellular environment of cells in various tissues. Like its protein family members, 14-3-3η adopts a homodimer conformation, is abundant in the human brain and possesses chaperone activity[38,50]. In NDs, this isoform is particularly interesting with regards to PD due to its association with αS and its effects on the aggregation process[38].

1.7.1 14-3-3η and its interactions with α-Synuclein

Unlike certain other 14-3-3η isoforms, immunostaining studies have not detected 14-3-3η in LBs of PD patients[49,51]. However, there are other indications that this isoform interacts with αS and is involved in the pathogenesis of PD. 14-3-3η was found to co-immunoprecipitate with αS from the substantia nigra of PD brains[52], indicating an association between the two proteins in the affected brain region. Furthermore, *in vitro* experiments with αS and 14-3-3η demonstrated that 14-3-3η associates with αS and forms tight complexes termed non-fibrillar products (NFPs)[9], a further indication that the two proteins interact (Figure 1.7). It is not yet clear as to which αS aggregation stage 14-3-3η binds, nor have the properties of a possible binding been reported. However, it has been suggested that 14-3-3η binds specifically to soluble αS oligomers[9]. Similarly, the binding mode through which 14-3-3η binds αS has yet to be characterized. The interaction does not appear to follow the canonical phospho-peptide binding mode, as 14-3-3η have been shown to interact with unphosphorylated αS[9]. Moreover, 14-3-3η, like all isoforms of the 14-3-3 family, also displays chaperone activity where the mode of binding is less characterized[44]. Taken together, these findings suggest an interaction between 14-3-3η and αS, and that this interaction could affect αS misfolding and further aggregation.
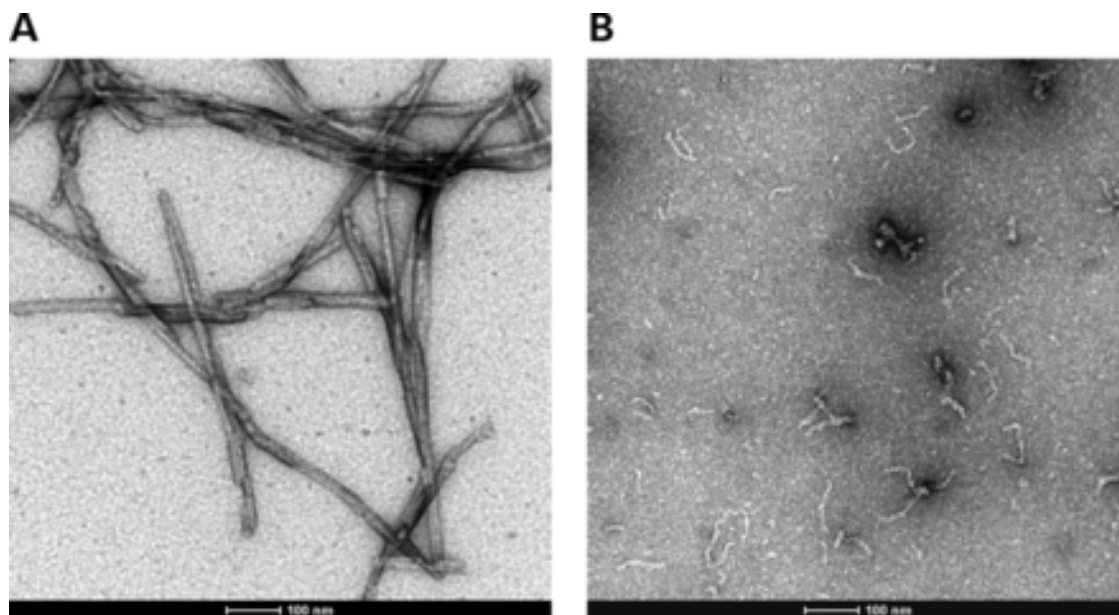
Figure 1.7 – TEM images of aggregated α-Synuclein (αS) fibrils and α-S/14-3-3η complexes. Experimental work by Plotegher *et al*[9] shows TEM images of mature αS fibrils obtained by aggregating αS alone (A), compared to the smaller, non-fibrillar products (NFPs) obtained by aggregating αS in the presence of 14-3-3η in a 4:1 ratio (B). Interaction with 14-3-3η during the aggregation process thus affects the αS aggregation pathway, rerouting it towards the smaller NFPs rather than mature fibrils. Figure from Plotegher *et al*[9].

1.7.2 The role of 14-3-3η in α-Synuclein aggregation and Parkinson's disease pathology

With regards to the αS aggregation process, *in vitro* fluorescence-monitored studies by Plotegher *et al*[9] showed that 14-3-3η was able to attenuate αS aggregation by reducing fibril formation, even when present in sub-stochiometric amounts of 4:1 (αS:14-3-3η). This study also implied that 14-3-3η interacts with oligomeric species of αS rather than monomers, leading to the formation of NFPs (Section 1.7.1) rather than canonical αS fibrils[9]. Hence, this points to a suppressing and neuroprotective role of 14-3-3η in fibril formation. Furthermore, these observations appeared to be isoform-specific to 14-3-3η. However, the suppressing effects of 14-3-3η ceased at a critical αS:14-3-3η ratio or when αS aggregation had already progressed to the later stages. In these conditions, 14-3-3η becomes sequestered into αS fibrils and are no longer able to affect the process[9]. Moreover, 14-3-3η is connected to PD in other aspects as well. Sato *et al*[52] showed that 14-3-3η binds to and regulates the activity of Parkin, a ubiquitin ligase which if mutated leads to early onset PD and is suggested to interact with αS[53]. Hence, overexpression of αS and its progressing aggregation could sequester 14-3-3η from the Parkin/14-3-3η complex, depriving the cells of regulatory processes. Interestingly, overexpressing 14-3-3η reduced αS-induced cellular toxicity in HEK293 cells overexpressing αS[9]. In summary, 14-3-3η could be a protein of interest in uncovering suppressors of αS aggregation and therapeutic targets in PD.

1.8 BIOPHYSICAL METHODS FOR STUDYING PROTEINS *IN VITRO*

In this thesis, several methods were employed to investigate protein interactions, structure and aggregation kinetics. Common to all these methods is their basis in biophysics. This section provides an overview of two key methods and their underlying principles.

1.8.1 Thioflavin T (ThT) monitored aggregation assays

Studies of aggregating proteins such as αS are often conducted *in vitro*, as a convenient means to investigate both aggregation kinetics and influencing factors. Such aggregation assays are commonly performed with the fluorescent dye named Thioflavin T (ThT)[54]. When existing freely in solution, ThT rotates around a central C–C bond, and exhibits weak fluorescent signals only when it enters a certain rotational position. Upon binding to the cross-β structure of amyloid fibrils however, this bond is immobilized. As a result, ThT becomes sterically locked in a position that emits a strong fluorescent signal with excitation and emission maxima at 450

nm and 480 nm, respectively[55]. ThT is thus a sensitive reporter of amyloid fibril formation and can be used to monitor αS fibril formation *in vitro*. ThT-monitored aggregation assays are normally performed in fluorescence plate-reader format, e.g. in a 384-well microplate, which allows multiple samples and conditions to be tested simultaneously (Figure 1.8)[54]. Protein samples with ThT, and possibly influencing factors, can then be exposed to aggregation-promoting conditions and monitored by measuring the fluorescence intensity of ThT over time. This yields a fluorescence curve whose intensity is proportional to the fibril formation over time, providing a starting point for assessing the kinetics of protein aggregation. However, fibril nucleation and growth are rather stochastic in nature. Consequently, these types of assays usually require multiple replicates and can be prone to poor reproducibility[54].
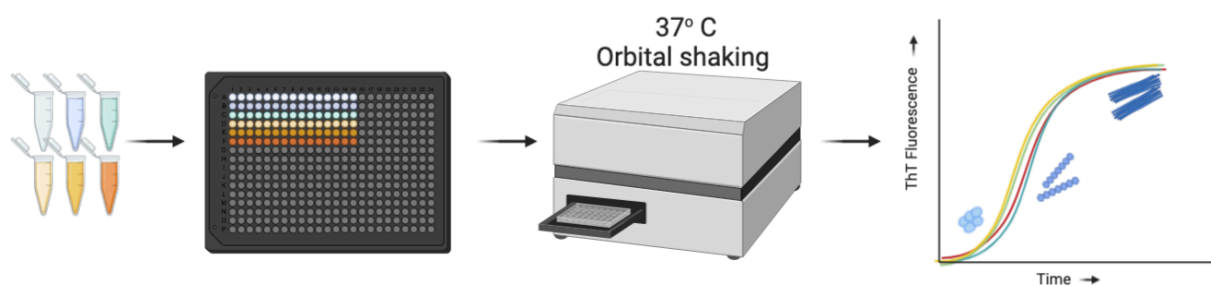
Figure 1.8 – ThT-monitored aggregation assays: experimental overview. Multiple samples of an amyloid protein mixed with ThT, and possibly aggregation-influencing factors, are pipetted into a microplate with several wells. A fluorescence microplate-reader set to aggregation-promoting conditions is then used to measure ThT fluorescence in the samples over time. Due to the fibril-dependent ThT-fluorescence, this yields a fluorescence curve which is proportional to the number of fibrils; the intensity increases as the aggregation process transitions from primary nucleation to fibril elongation and finally the plateau phase of fibrils only. Figure created in BioRender.com.

1.8.2 Nuclear magnetic resonance (NMR) spectroscopy

When subjected to a strong magnetic field and electromagnetic pulse, NMR active nuclei ^{1}H, ^{13}C and ^{15}N emit resonance signals of varying frequencies as they transition between energy levels. These signal frequencies are Fourier-transformed to chemical shifts (δ [ppm]), which differ between the nuclei depending on the atoms surrounding them, i.e. their position in a molecule. These signals can then be detected and processed into spectra which give information about protein structure[56]. Moreover, nuclei linked either through-bond or through-space can exchange excitation energy, yielding correlated signals termed cross-peaks. In protein biochemistry, this has proven incredibly useful. Depending on the type of experiment and the isotope-labeling of a protein, two-dimensional (2D) or three-dimensional (3D) spectra can be acquired from a protein sample. Subsequently, the cross-peaks of specific δ-values can be

exploited to determine structural information about the protein, such as size, backbone residues, information about neighboring residues and indications of the protein fold[57]. As an example, ^{1}H-^{15}N heteronuclear single quantum coherence spectroscopy (HSQC) can be used to detect N-H bonds in the backbone peptide bonds. Therefore, NMR spectroscopy has become an integrated part of structural molecular biology and can even be employed when investigating protein-protein interactions[56]. However, NMR spectroscopy has its limitations; structures of large proteins are still challenging to solve, due to their great number of nuclei and fast relaxation rates creating complex spectra[58]. With more recently developed techniques such as transverse relaxation optimized spectroscopy (TROSY), this size limit has greatly increased[58] but remains a challenge.

1.9 AIMS AND OBJECTIVES OF THE STUDY

To this day, there is no early diagnostic method nor effective treatments for PD[7,8]. However, fibrillar products of αS have been discovered as the primary component of LBs; insoluble inclusions found in parkinsonian brains[9,10]. The misfolding and aggregation of this small synaptic protein is therefore deemed of great importance in the PD pathogenesis. Several proteins are now evaluated and researched as potential suppressors of these mechanisms. In this context, the 14-3-3 family of chaperone-like proteins have received attention in the search for neuroprotective factors and possible therapeutic targets[9,47]. In particular, the 14-3-3η isoform shows promise as a modulator of αS aggregation, and a possible rescuer of αS-induced cellular toxicity[9]. Uncovering the role of 14-3-3 proteins in PD could therefore be important in understanding the disease pathogenesis and in the search for therapeutic targets. In this study, we aim to elucidate the effects of 14-3-3η on PD-related αS aggregation and characterize the interaction between the two proteins based on the following hypotheses:

1. The presence of 14-3-3η influences αS aggregation kinetics and could be part of a proteostasis network which counteracts aggregation processes harmful to cells.
2. 14-3-3η interacts with αS only at certain aggregation states through a non-canonical binding mode for 14-3-3 proteins.

2. MATERIALS

2.1 CHEMICALS

Table 2.1: Chemicals and reagents used in various experiments

Chemical	Formula	Supplier	#Cat. Number
10 % Ammonium Persulfate	APS	Sigma	-
Ampicillin Sodium Salt	Ampicillin	Sigma	A0166
Benzamidine	-	Sigma	B-6506
Chloramphenicol	$C_{11}H_{12}C_{l2}N_2O_5$	Sigma	C0378
cOmplete, EDTA-free: protease inhibitor cocktail tablets	EDTA-free protease inhibitors	Roche Diagnostics	-
DL-dithiothreitol	DTT	Merck	D9163
Ethylenedinitrilotetraacetic acid	EDTA	Merck	1.08418.1000
Glucose	$C_6H_{12}O_6$	Sigma	49159
Glutathione	-	Sigma	G4251
Glycine	$C_2H_5NO_2$	Sigma	G8898
Hydrochloric acid	HCl	-	-
Imidazole	$C_3H_4N_2$	Sigma	792527
Isopropyl 1-thio-β-D-galactopyranoside	IPTG	Sigma	I5502
Lysogeny Broth-Agar	LB-Agar	Sigma	L2897
Magnesium Chloride	$MgCl_2 \bullet 6H_2O$	Merck	1.05833.1000
Magnesium Sulfate	$MgSO_4$	Sigma-Aldrich	M-7506
Peptone (Tryptone)	-	Merck	1.07213.1000
Potassium Chloride	KCl	Merck	1.04936.1000
Saccharose	$C_{12}H_{22}O_{11}$	Sigma	S9378
Sodium Azide	NaN_3	-	-
Sodium Chloride	NaCl	VWR Chemicals	27810.295
Sodium dihydrogen phosphate, monobasic	$NaH_2PO_4 \bullet H_2O$	Sigma	71662
Sodium hydrogen phosphate, dibasic	$Na_2HPO_4 \bullet 2H_2O$	Sigma	71504
20% Sodium Dodecyl Sulfate	SDS	Alfa Aesar	J63394
Sodium Oxide	NaOH	-	-
N,N,N',N'-tetramethylethane-1,2-diamine	TEMED	Sigma	T9281
Thioflavin T	ThT	Sigma	T3516
TPE-TPP	-	-	-
Trizma Base	Tris	Sigma	T1503
Yeast Extract (granulated)	-	Merck	1.03753.0500

2.2 ISOTOPES

Table 2.2: Isotopes used for labeled protein expression

Isotope	Formula	Supplier	#Cat. Number
^{13}C D- glucose	$^{13}C_6H_{12}O_6$	Cambridge Isotope Laboratories	CLM-1396-1
^{15}N-ammonium chloride	$^{15}NH_4Cl$	Sigma	299251
Deuterium Oxide	D_2O	Cortecnet	D214K

2.3 PLASMIDS AND PRIMERS

Table 2.3a: Plasmids used for sequencing and expression

Plasmid	Supplier	#Cat. Number
pET21a-α-Synuclein	AddGene	51486
pGEX-2T-14-3-3η	Kind gift from Dr. Rune Kleppe	-

Table 2.3b: Primers used for sequencing

Primer	Sequence (5' - 3')	Supplier
pGEX 2TSeq	ATATAGCATGGCCTTTGCAG	Sigma
T7 Terminal primer	GCTAGTTATTGCTCAGCGG	Addgene

2.4 ENZYMES, PROTEINS AND CELLS

Table 2.4: Enzymes, proteins and cells

Name	Application	Supplier
Benzonase Nuclease	Cell lysis	Sigma
BL21 Star™ (DE3) Chemically Competent *E. coli*	Protein Expression	ThermoFisher Scientific
Bovine Serum Albumin (BSA)	Aggregation assays	Sigma
Bovine Serum Albumin (BSA), fatty acid (FA)-free	Aggregation assays	Sigma
Lysozyme from chicken	Cell lysis	Sigma
Thrombin	14-3-3η cleavage	-
Tobacco Etch Virus (TEV) Enzyme	αS cleavage	-

2.5 COMMERCIAL REAGENTS, MATERIALS AND KITS

Table 2.5: Commercial reagents and materials

Material	Application	Supplier
10X HBS-EP+ buffer	SPR interaction studies	GE Healthcare
384-well black microplate, clear bottom	Aggregation assays	Corning
Acrylamide-Bisacrylamide 30% 37.5:1	SDS-PAGE	Sigma
Amicon 10 kDa Centrifugation filter	Up-concentrating proteins	Millipore
BME Vitamins Solution 100x	Isotope-labeled protein expression	Sigma-Aldrich
Glutathione-Sepharose 4B Resin	Protein purification	GE Healtchare
HiLoad 16/600 Superdex 75 pg	Protein Purification	GE Healthcare
HiTrap Hp 5mL	Protein purification	GE Healthcare
Immobilization buffer (Acetate buffer) pH 4.0	SPR interaction studies	GE Healthcare
Instant Blue™ Protein Stain	Visualization of proteins	Expedeon
Precision Plus Protein DualColor Standard	Protein marker	Bio-Rad

2.6 INSTRUMENTS AND EQUIPMENT

Table 2.6: Instruments and equipment

Instrument	Application	Manufacturer
AEKTA Explorer	Protein purification	GE Healthcare
Biacore T200	SPR interaction studies	GE Healthcare
Bruker Advanced	NMR Experiments	Bruker
FLUOStar Optima	Aggregation assays	BMG Labtech
GelDoc™ XR+	Gel Imaging	Bio-Rad

2.7 COMPUTER SOFTWARE

Table 2.7: Computer software and web resources

Software	Application	Manufacturer
MatLab R2018b	Processing fibrillation curves	MathWorks
TopSpin 4.0.7	Processing NMR spectra	Bruker
Pint	Analyzing NMR spectra	Pint
Biacore Evaluation Software	Evaluating SPR results	GE Healthcare
ImageLab 5.2.1	Processing Gel images	BioRad
BioRender.com	Creating figures	BioRender

2.8 BUFFERS, MEDIA AND SOLUTIONS

MilliQ Ultrapure water was used in all buffers and solutions unless otherwise stated.

2.8.1 Buffers and solutions for protein expression

LB-agar
37 g/L LB-Agar Broth

Lysogeny broth (LB) medium
10 g/L Peptone (Tryptone)
5 g/L Yeast Extract (granulated)
10 g/L NaCl

Ampicillin stock solution
100 mg/ml Ampicillin Sodium Salt

Chloramphenicol stock solution
34 mg/ml Chloramphenicol
(Dissolved in 70% ethanol)

IPTG stock solution
1M IPTG

SOC medium
0.5 % Yeast Extract
2 % Tryptone
10 mM NaCl
2.5 mM KCl
10 mM $MgCl_2$
10 mM $MgSO_4$
20 mM Glucose

2.8.2 Buffers and solutions for isotope-labeled protein expression

5X M9 Salts (filtered)
110 mM KH_2PO_4
240 mM Na_2HPO_4
2.5 g/L NaCl
5 g/L $^{15}NH4CL$

5X M9 Salts Wash (filtered)
110 mM KH_2PO_4
240 mM Na_2HPO_4
2.5 g/L NaCl

1L 5M Modified minimal medium (filtered)
200 mL 5XM9 Salts
4 g D-Glucose ^{13}C
2.5 mL 100X BME Vitamins
2.0 mL 1M $MgSO_4$
1 mL/L Trace Metal Solution
(Dissolved in D_2O when used for triple-labeled expression)

2.8.3 Buffers and solutions for protein purification

Osmotic shock buffer
30 mM Tris-HCl pH 8
40% w/v Saccharose
2 mM EDTA

HisTrap wash buffer (filtered)
20 mM Tris-HCl pH 8.0
150 mM NaCl
20 mM Imidazole

10 X PBS pH 7.3 (filtered)
100 mM $Na_2HPO_4 \bullet 2H_2O$
18 mM KH_2PO_4
1.4 M NaCl
27 mM KCl

HisTrap elution buffer (filtered)
20 mM Tris-HCl pH 8.0
150 mM NaCl
500 mM Imidazole

Cell lysis Buffer
1 X PBS
1 mM EDTA
1 mM DTT
1/50 mL EDTA-free protease inhibitor tablets
10 mM Benzamidine
1U/ml Benzonase
0.5 mg/ml Lysozyme

TEV cleavage buffer
20 mM Tris-HCl pH 8
150 mM NaCl
0.5 mM EDTA
1 mM DTT

1 M Sodium phosphate buffer pH 7.4
0.612 M $Na_2HPO_4 \bullet 2H_2O$
0.388 M $NaH_2PO_4 \bullet H_2O$

1 M sodium phosphate buffer pH 6.0
0.13 M $Na_2HPO_4 \bullet 2H_2O$
0.87 M $NaH_2PO_4 \bullet H_2O$

GST elution buffer
50 mM Tris-HCl pH 8.0
20 mM Glutathione
1 mM DTT

2.8.4 Buffers and solutions for Sodium dodecyl sulphate polyacrylamide gel electrophoresis (SDS-PAGE)

SDS-PAGE electrophoresis buffer pH 8.3
192 mM Glycine
25 mM Tris
0.1 % w/v SDS

4X SDS Sample buffer
200 mM Tris HCl pH 6.8
17% Glycerol
4% SDS
10% β-mercaptoethanol
0.005% Bromophenol blue
0.0005 % Pyronin B

2 x 0.75 mm 4% SDS-PAGE stacking gel
125 mM Tris-Glycine pH 6.8
4% Acrylamide-Bisacrylamide
0.1% SDS
0.05% APS
0.1% TEMED

2 x 0.75 mm 13% SDS-PAGE resolving gel
375 mM Tris-Glycine pH 8.8
13% Acrylamide-Bisacrylamide
0.1% SDS
0.05% APS
0.05% TEMED

2.8.5 Buffers for nuclear magnetic resonance spectroscopy

NMR buffer pH 6.0
20 mM sodium phosphate pH 6.0
100 mM NaCl
0.02% w/v NaN_3

NMR buffer pH 6.8
20 mM sodium phosphate pH 6.8
100 mM NaCl
0.02% w/v NaN_3

NMR buffer pH 7.4
20 mM sodium phosphate pH 7.4
100 mM NaCl
0.02% w/v NaN_3

2.8.6 Thioflavin T (ThT) monitored α-Synuclein aggregation assays

PB buffer no salt
20 mM sodium phosphate pH 6.0
1 mM EDTA
0.02% NaN_3

PB buffer w/salt
20 mM sodium phosphate pH 6.0
1 M NaCl
1 mM EDTA
0.02% NaN_3

ThT Pre-stock Solution
8.5 M ThT

ThT Stock Solution (filtered)
1 mM ThT

3. METHODS

The primary goal of this thesis was to employ ThT-monitored aggregation assays to investigate how 14-3-3η affects the kinetics of αS aggregation *in vitro*, and further characterize the binding between 14-3-3η and αS by NMR spectroscopy and surface plasmon resonance (SPR) experiments.

3.1 α-SYNUCLEIN EXPRESSION AND PURIFICATION

3.1.1 α-Synuclein expression

Sequencing of the pET21a-α-synuclein plasmid was performed to check for plasmid mutations that may affect the translated protein, following the BigDye v.3.1 Protocol. *E. coli* BL21 (DE3) Star chemically competent cells were incubated 15 min on ice, then transformed with 6xHis-tagged pET21a-α-synuclein (Addgene) with a TEV cleavage site. After additional 30 min ice incubation, heat-shock was applied for 30 sec at 42°C to enable uptake of plasmid DNA, followed by 2 min ice incubation before the cells recovered in 250 μl SOC medium. Bacterial colonies grew overnight on LB-Agar plates w/Ampicillin (100 μg/ml), and a single colony was used to inoculate a starter-culture of LB medium. Bacterial growth occurred in 4 L LB-medium w/Ampicillin (100 μg/ml) at 37°C and 250 rpm until OD = 0.4, upon which αS expression was induced by addition of 0.1 mM IPTG. The protein was expressed in culture for 5 hours (37°C and 250 rpm).

3.1.2 Extraction of periplasmic content

Bacteria were harvested by centrifugation (15 000 g, 4°C, 20 min), and the cell pellet resuspended in Osmotic shock buffer (250 mL/L of original culture). Subsequently, the resuspension was incubated at room temperature (10 min) before harvest by centrifugation (15 000 g, 4°C, 20 min) to obtain a new pellet of 4X concentrated cells. This pellet was resuspended in cold 1mM $MgCl_2$ before the periplasmic content (PC) was recovered by centrifugation (15 000 g, 4°C, 20 min) as a supernatant. To inhibit proteolytic cleavage, 20 mM sodium phosphate buffer pH 7.4 w/EDTA-free protease inhibitors was added to PC prior to further purification.

3.1.3 Chromatography purification

Exploiting the affinity of the 6xHis-tag imidazole rings to Ni^{2+} ions, αS was purified from the PC by HisTrap affinity chromatography (AEKTA Explorer system, GE Healthcare), using

HiTrap HP 5mL columns. Non-specific proteins were eluted with HisTrap wash buffer before elution of αS was induced by increasing concentrations of HisTrap elution buffer (flowrate 0.5 ml/min), while monitoring protein fractions with UV_{280} absorbance. Subsequently, the αS buffer was exchanged to TEV Cleavage buffer (20 mM Tris-HCl pH 8, 150 mM NaCl, 0.5 mM EDTA, 1 mM DTT) using PD10 columns, before overnight cleavage at 4°C with $1mg/50mg_{αS}$ of TEV (purified locally) to remove the His-tags. A second affinity chromatography was used to purify cleaved αS as column flow-through. Eluted protein was concentrated with a 10 kDa spin column (Amicon Ultra, Millipore). αS was further purified by running size-exclusion chromatography (SEC, AEKTA Explorer system), using the HiLoad Superdex 75 pg 16/600 column with 20 mM sodium phosphate pH 6.0 w/ 100 mM NaCl (flowrate 1.0 ml/min). Purified αS was stored at -80°C until use.

3.2 14-3-3η EXPRESSION AND PURIFICATION

3.2.1 14-3-3η Expression

Sequencing of the expression vector pGEX-2T-14-3-3η was performed to check for mutations that may affect the translated protein, following the BigDye v.3.1 Protocol. *E. coli* BL21 (DE3) Star chemically competent cells were transformed with GST-tagged pGEX-2T-14-3-3η with a Thrombin cleavage site, by the procedure described in Section 3.1.1. Colonies grew overnight in LB-Agar plates w/Ampicillin (50 μg/ml) and Chloramphenicol (34 μg/ml), and a starter-culture was inoculated with a single colony. Growth occurred in 2L LB-medium w/Ampicillin (100 μg/ml) and Chloramphenicol (34 μg/ml) at 37°C and 250 rpm, and protein expression was induced with 1 mM IPTG at OD=0.8. Based on testing of various expression conditions, 14-3-3η was expressed in culture at 25°C and 250 rpm overnight to achieve optimal yield.

3.2.2 Cell lysis

Bacteria were harvested by centrifugation (15 000 g, 4°C, 20 min) and the cell pellet resuspended in Cell lysis buffer (1 X PBS, 1 mM EDTA, 1 mM DTT, 1/50 mL EDTA-free protease inhibitors, 10 mM Benzamidine, 1U/ml Benzonase, 0.5 mg/ml Lysozyme). Cells were then lysed by sonication (50% amplitude, 30 sec on/15sec off, 10 min), centrifuged (15 000 g, 4°C, 20 min) and the cell lysate (CL) collected in the supernatant.

3.2.3 Chromatography purification

GST-tagged 14-3-3η was purified from CL by GST-Glutathione affinity chromatography using a Glutathione-Sepharose resin (6 ml). The column was equilibrated with three column volumes (CV) of 1XPBS w/protease inhibitors (10 mM Benzamidine and 1 EDTA-free protease inhibitor tablet), before CL was added on the glutathione resin and incubated at for 30 min at 4°C. The lysate/resin was washed with 3 CV of 1XPBS w/protease inhibitors to remove unspecific proteins. Subsequently, the column was washed with 3 CV of 1XPBS and resuspended in 1 CV 10 U/ml Thrombin in 1XPBS (expressed locally) for incubation overnight (4°C, w/shaking) to remove the GST tag. 14-3-3η was eluted with 1XPBS and collected in 0.5-1.5 ml fractions, and the column was equilibrated with GST Elution buffer and 20% ethanol. Fractions of 14-3-3η with $Absorbance_{280}$ > 0.5 were pooled and up-concentrated in a 10 kDa Spin Column (Amicon Ultra, Millipore). SEC was performed as the final purification step on the HiLoad Superdex 75 pg 16/600 column as described in Section 3.1.3, and the protein was stored at -80°C until use.

3.3 EXPRESSION OF ISOTOPE-LABELED α-SYNUCLEIN AND 14-3-3η

E. coli BL21 (DE3) Star chemically competent cells were transformed with pET21a-α-synuclein and pGEX-2T-14-3-3η and cells grown in 4L LB medium as described in Sections 3.1.1 and 3.2.1 until OD=0.4 and 0.8. Cells were harvested by centrifugation (15 000 g, 4°, 20 min) and resuspended in 5X M9 Salts Wash (250 ml/L original culture) before a second centrifugation (15 000 g, 4°C, 20 min) to obtain a 4X concentrated cell pellet. The 4X concentrated cells were then resuspended in 1L 5 M Modified minimal medium containing ^{15}N-ammonium chloride and ^{13}C-glucose (and D_2O for triple-labeled expression), then incubated at 37°C, 250 rpm for one hour. Subsequently, expression of the isotope-labeled proteins was induced as in Sections 3.1.1 and 3.2.1. Purification was performed as in Sections 3.1.3 and 3.2.3.

3.4 SODIUM DODECYL SULPHATE POLYACRYLAMIDE GEL ELECTROPHORESIS

To evaluate the degree of protein purity, samples from the purification processes (Sections 3.1, 3.2, 3.3) were analyzed by sodium dodecyl sulphate- polyacrylamide gel electrophoresis (SDS-PAGE). Samples were prepared by adding 1X SDS sample buffer followed by incubation at 95°C for 5 min to achieve protein denaturation. In volumes ranging from 3-20 μL, samples

were loaded on a 13 % polyacrylamide gel (4 % stacking gel), using Precision Plus Protein Standard™ DualColor (BioRad) as size marker. Electrophoresis ran at 80-120 V until satisfactory separation was obtained. Proteins were subsequently stained with Instant Blue™ Protein Stain (Expedeon) for 15 min and visualized with GelDoc™ XR+ (BioRad).

3.5 NUCLEAR MAGNETIC RESONANCE SPECTROSCOPY

3.5.1 Sample preparation

Three 180 μM $^{13}C^{15}N$-labeled αS samples were prepared in NMR buffer (20 mM sodium phosphate, 100 mM NaCl, 0.02% NaN_3) with pH 6.0, 6.8 and 7.4, supplemented with 5% D_2O and pipetted into NMR tubes in volumes of 300 μL. One sample of 264 μM $^{13}C^{15}N$-labeled 14-3-3η was prepared in NMR buffer pH 6.0, supplemented with 5% D_2O before 300 μL was pipetted into the NMR tube. One sample of approximately 50 μM $^{2}H^{13}C^{15}N$-labeled 14-3-3η was prepared in NMR buffer pH 6.0, supplemented with 5% D_2O before 500 μL was pipetted into the NMR tube.

3.5.2 Acquisition and Processing

Data were collected at 25°C on an 850 MHz Bruker Advanced III HD Spectrometer fitted with a $^{1}H^{13}C^{15}N$ TCI CryoProbe and a SampleJet with temperature control for storing samples between runs (set to 4°C). Prior to data acquisition, the instrument was locked onto D_2O in the sample, tuned and matched. Samples were shimmed using the automated gradient shimming protocol "TopShim", while probe- and solvent specific parameters were set with the "getprosol" command. Gradients were set with the "gppp" command. For 2D experiments, only the number of scans (ns) and the number of transients in the artificial time domain(s) (TD1, TD2) were typically adjusted. Datasets were processed into the final spectra in TopSpin 4.0.7. Linear prediction up to twice the number of acquired points were performed in the artificial time domains to improve resolution. Datasets were processed using square cosine functions for apodization of the acquired free induction decays, yielding better baselines and enhanced signals.

3.5.3 NMR Experiments

Table 3: List of NMR Experiments

NMR Experiment	Pulse Sequence (Bruker Designation)	Spectral Width in each dimension (SW, ppm)	Number of complex points in each dimension (TD)	Number of scans per experiment (NS)	Sample
^{1}H^{15}N-HSQC	hsqcetf3gpsi	7.9911, 35.0001	2048, 256	10	180 μM ^{13}C^{15}N-αS
^{1}H^{15}N-HSQC	hsqcetf3gpsi	7.9911, 35.0001	2048, 256	10	264 μM ^{13}C^{15}N-14-3-3η
^{1}H^{15}N-HSQC	hsqcetf3gpsi	14.0034, 35.0001	2048, 128	224	50 μM ^{2}H^{13}C^{15}N-14-3-3η
^{1}H^{15}N-TROSY-HSQC	trosyetf3gpsi	17.9312, 35.0000	2048, 128	224	

3.6 THT-MONITORED α-SYNUCLEIN AGGREGATION ASSAYS

The β-sheet fibril-dependent fluorescence of ThT was used to monitor αS aggregation in the absence and presence of 14-3-3η. All fluorescence readings were performed with FLUOStar Optima Microplate Fluorescence Reader, using a black 384-well polystyrene microplate with clear bottom, sealed with sealing tape to avoid evaporation of samples. Excitation and emission wavelengths were set to 430 nm and 485 nm for ThT, and the fluorescence gain was set to 20%.

3.6.1 Optimizing salt concentrations

To find the optimal buffer salt concentration, samples were prepared in PB buffer pH 6.0, with fixed concentrations of 5μM ThT, 60 μM αS and varying NaCl concentrations of 100, 200 and 500 mM NaCl. Additionally, a ThT blank was prepared in PB buffer w/100 mM NaCl. The assay was performed with 20 wells/sample and 50 μL/well. At 37 °C, fluorescence was measured in time intervals of 700 s, with 300 s and 7 mm orbital shaking, for 140 hours.

3.6.2 Investigating the influence of 14-3-3η on α-Synuclein aggregation

Samples were prepared in PB buffer pH 6.0 with fixed concentrations of 200 mM NaCl, 5μM ThT, 100 μM αS and varying concentrations of 14-3-3η (0, 10, 20 and 55 μM). An additional sample with αS and 55 μM BSA or fatty acid-free (FA-free) BSA was prepared as controls. The assay was performed with 15 wells/sample and 50 μL/well. Fluorescence was measured at

37°C, in 700 s cycles with 300s and 2 mm orbital shaking, for 140 hours. Five independent replicates were performed with αS and 14-3-3η to achieve increased reliability of the results, but only three replicates with αS + BSA and αS + FA-free BSA could performed within the time restrictions of the project. The recorded fluorescence data were processed in MatLab R2018b, using an in-lab written script. The resulting fluorescence curves were fitted to the two-step model in Equation 1, 2 to obtain lag times, t_n, and rate constants, v, for αS aggregation. Additionally, they were further processed in a cumulative aggregation analysis, evaluating the percentage of wells with a signal above a threshold of three times higher than the noise.

$$F(t) = \frac{1}{1 + e^{\frac{-4v(t-t_1)}{2}}} \qquad (1)$$

$$t_n = t_{1/2} - \frac{1}{2v} \qquad (2)$$

3.7 SURFACE PLASMON RESONANCE (SPR) INTERACTION STUDIES

By detecting small changes in the refractive index of thin films on sensor chips, SPR is used as a highly sensitive method for monitoring protein-protein interactions, and was therefore used to investigate the binding between 14-3-3η and αS. The method is based on the generation of a surface plasmon wave (a collection of conducting electrons), which changes the angle and intensity of reflected light, depending on the molecular mass of the sensor chip. An analyte protein binding to or dissociating from a ligand immobilized to the chip surface will change the surface molecular mass, and thus change the angle of reflected light. This change is detected in arbitrary response units (RU), used to evaluate the properties of the interaction[59].

Studies were performed with the BiaCore T200 instrument, in HBS-EP+ buffer (GE Healthcare). To investigate the binding of αS and 14-3-3η, αS was covalently linked by standard amine coupling to a CM5 sensor Chip. The flow cell system was primed with HBS-EP+ buffer, then pre-conditioned with HBS-EP+, 100 mM HCl, 50 mM NaOH and 0.5 % SDS prior to activation with 1-ethyl-3-(3-dimethylaminopropyl) carbodiimide (EDC) and N-hydroxysuccinimide (NHS). Monomeric αS (50 μg/ml), filtered to avoid oligomer contamination, was immobilized to the chip on flow path 2 via amino coupling, in 10 mM acetate buffer with pH adjusted to 3.7, to a final density of 1900 response units (RU). Flow paths 1 and 2 were then blocked with ethanolamine to prevent non-specific binding, leaving

flow path 1 as a reference. Non-specifically immobilized ligand was removed from the CM5 chip by washing for several hours at 50 µl/min with HBS-EP⁺ running buffer prior to SPR analysis. Experiments were performed at 25 °C in running buffer at a flow rate of 25 µl/min. Subsequently, 14-3-3η in concentrations of 0.5, 1.0, 2.5, 5.0 and 10 µM was used for binding analysis, with 240 s contact time, 600 s dissociation time and a 30 s stabilization period. 10 mM Glycine pH 2.2 at 30 µl/min was used to regenerate the chip between each concentration. A blank run with HBS-EP⁺ buffer was subtracted from all curves after removing the signal from the reference cell. The resulting sensorgrams were evaluated in BiaCore evaluation software (GE Healthcare) to assess the properties of the interaction.

4. RESULTS

4.1 PROTEIN EXPRESSION AND OPTIMIZATION

4.1.1 α-Synuclein expression and purification

To prepare protein material for use in aggregation experiments and interaction studies with 14-3-3η, recombinant αS was overexpressed in *E. coli* and purified by two-step column chromatography. After expression and purification, pure protein was achieved in yields of 10-12 mg from 4 L bacterial culture. The protein eluted as a single peak at a 60 ml elution volume, but with a shoulder towards higher elution volumes (Figure 4.1, a). αS is a small protein and was thus expected to elute at higher elution volumes, which could indicate that the presence of oligomers. However, αS has previously been found to migrate as a 57-60 kDa protein, rather than its actual size of 14 kDa, due to its intrinsically disordered and extended conformation.[60] It is therefore possible that the larger peak represents monomeric αS, and the shoulder towards higher elution volumes could represent a minor amount of oligomeric species, migrating as their actual size.

After cleavage by TEV, the His-tag which enabled αS to bind the Ni^{2+} matrix was successfully removed, seen by the decrease in protein size from 16.8 kDa to 14.9 kDa (Figure 4.1, b), the latter corresponding to the size of monomeric αS. However, as oligomers would present as monomers in a denatured protein solution, oligomer contaminations could have been present. Furthermore, a clear increase in purity of αS was observed after the 2nd HisTrap chromatography, however, some minor contaminations were still present in the sample, as seen in the gel sample from the 2nd round of HisTrap purification (Figure 4.1, b). Therefore, a final polishing step of SEC proved necessary in order to achieve the desired purity, with αS displayed as a single peak in the elution profile (Figure 4.1, a).
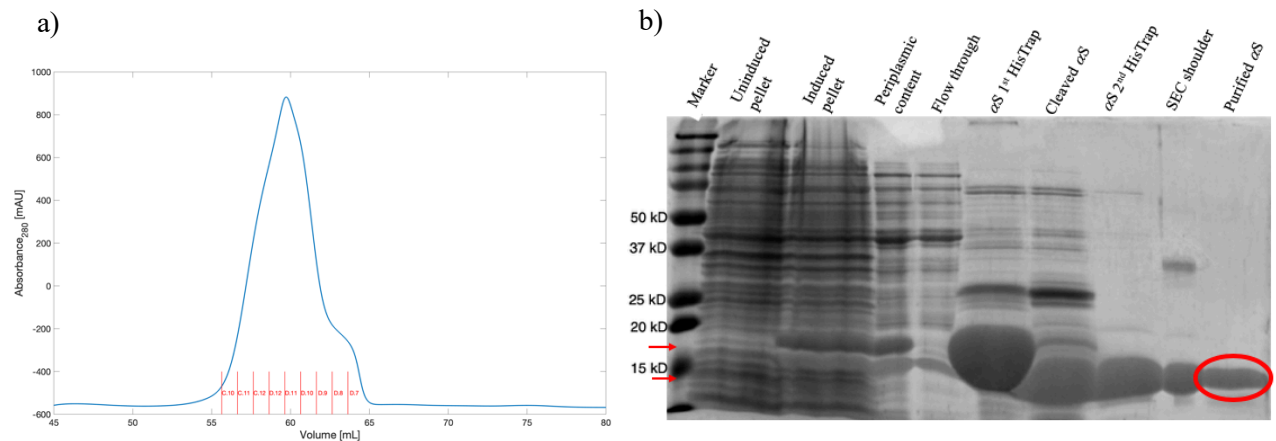
Figure 4.1 – Purification of recombinant α-Synuclein (αS). αS was expressed in *E. coli* BL21 (DE3) Star and purified by a two-step column chromatography, exploiting the affinity of a His-tag to a Ni^{2+} matrix, followed by subsequent SEC on the HiLoad Superdex 75 pg 16/600 column to achieve the highest possible purity. a) The SEC elution profile displayed one asymmetric peak, representing monomeric αS in the final sample. b) Samples from the purification process analyzed by SDS-PAGE revealed a clear increase in purity from the pellet of induced culture to the final purified product (circled), as well as a decrease in size from 16.8 kDa to 14.9 kDa upon cleavage of the His-tag (red arrows).

4.1.2 14-3-3η Expression and purification

In order to perform binding and aggregation experiments investigating the effect of 14-3-3η on αS, a recombinant 14-3-3η expression system (a gift from Dr. Rune Kleppe) was established and optimized. The protein was overexpressed in *E. coli* using a pGEX-2T-14-3-3η expression vector and purified by GST-glutathione affinity chromatography. Three different expression conditions were tested to optimize the method: 37°C for 4 hours, 30°C for 4 hours and 25°C overnight. SDS-PAGE analysis of the induced cultures indicated no differences in protein yield, and expression at 25°C overnight was therefore deemed the most convenient. Further optimization of the purification procedure revealed that a Glutathione resin and manual monitoring of the chromatography was preferable to using the automated AEKTA Explorer system and pre-packed columns.

Expression at 30°C for 4 hours and purification with the automated chromatography system yielded three peaks in the SEC elution profile (Figure 4.2, a), suggesting protein of lower purity, with contaminations corresponding to the size of GST (Figure 4.2, b). While keeping the same expression conditions and decreasing the flowrate of the automated chromatography system did improve purity, two peaks were still seen in the SEC elution profile (Figure 4.2, c). Expression at 25°C overnight and purification by automated chromatography with the decreased flow rates improved the purity to one elution peak (Figure 4.2, d), however, the protein yield was low.

Therefore, we opted to express 14-3-3η at 25°C overnight and purify the protein by manual chromatography with a glutathione resin to bind more protein to the column.
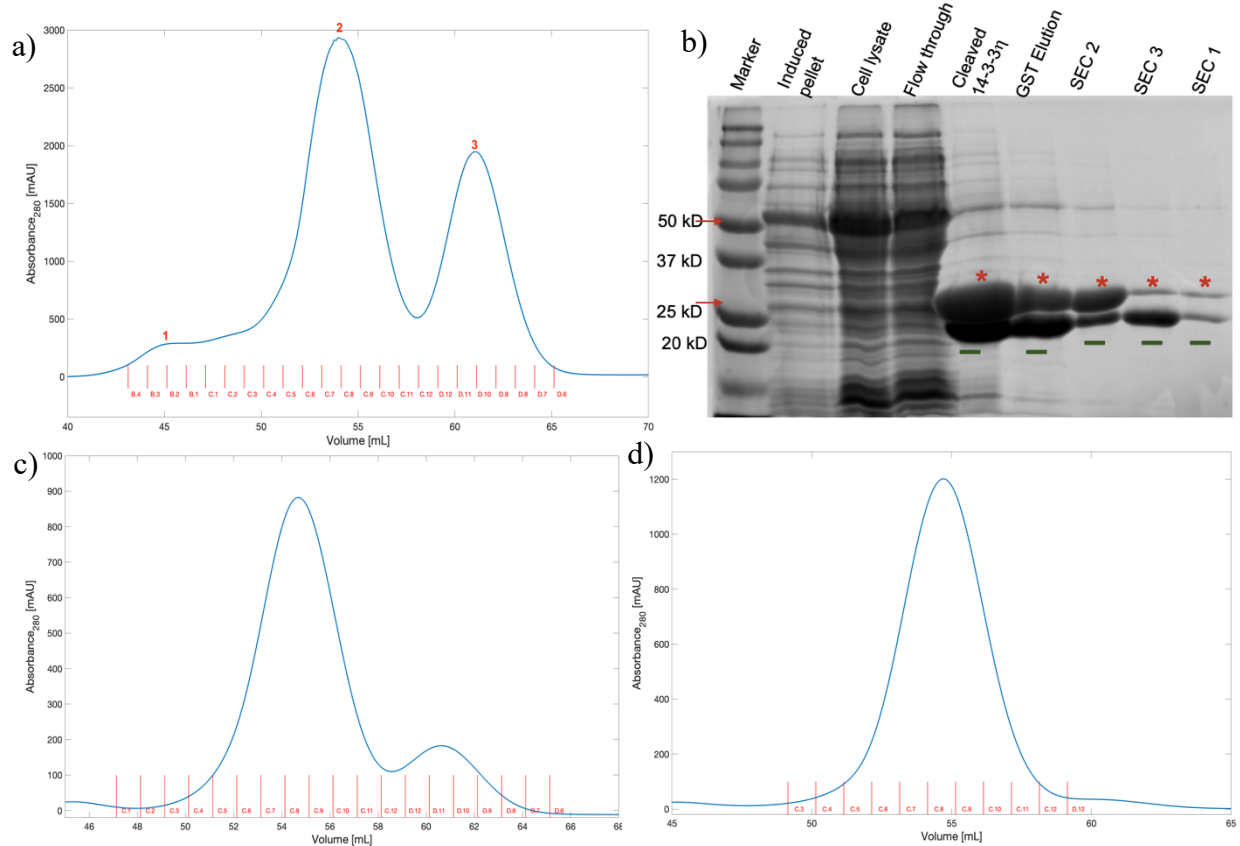
Figure 4.2 – Optimization of 14-3-3η expression conditions and purification. 14-3-3η was overexpressed in *E. coli* BL21 (DE3) Star in various conditions and purified with the AEKTA Explorer system. a) Expression at 30°C for 4 hours and purification with AEKTA Explorer yielded three peaks in the elution profile. b) Analysis by SDS-PAGE revealed that contaminations were likely cleaved GST (**--**) eluted with 14-3-3η (*****). c) Expression at 30°C for 4 hours, and lowered flowrates in the AEKTA system improved purity, but still yielded two peaks in SEC elution profile. d) Expression at 25°C overnight and lowered flowrates yielded pure protein, but low yield.

Using these methodological adaptations, GST-Glutathione chromatography and subsequent SEC yielded one peak in the SEC elution profile (Figure 4.3, a) and one 28 kDa protein band in SDS-PAGE analysis (Figure 4.3, b), indicating a high degree of 14-3-3η purity. Moreover, the protein eluted at a ~55 mL elution volume. Because this volume was expected for a protein twice the size of 14-3-3η monomers, this indicated that 14-3-3η was eluted in the dimeric conformation. With this optimized method, up to 28 mg dimeric 14-3-3η was obtained from 2 L bacterial culture.
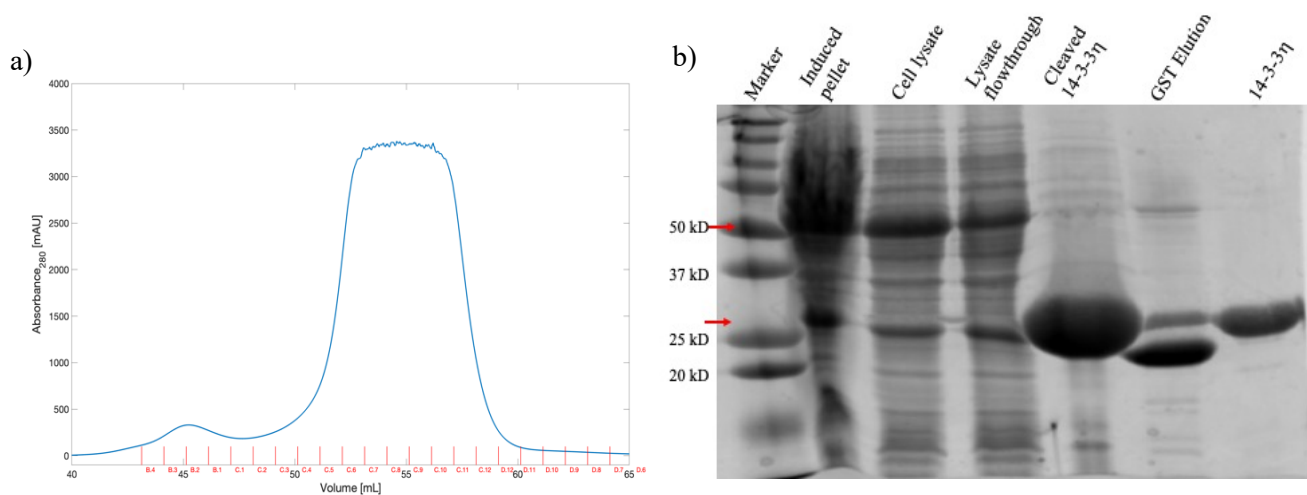
Figure 4.3 – Purification of recombinant 14-3-3η. 14-3-3η expressed in *E. coli* BL21 (DE3) Star was purified by GST-glutathione affinity chromatography and subsequent SEC on the HiLoad Superdex 75 pg 16/600 column, yielding 14-3-3η of high purity. a) The elution profile from final SEC purification yielded one peak, representing the pure 14-3-3η. b) SDS-PAGE analysis revealed a decrease in size from ~50 kDa prior to cleavage of the GST tag, to the final size of 28 kDa in the cleaved sample (red arrows). Contaminations in the cleaved sample were successfully removed by subsequent SEC to yield the fully purified 14-3-3η, as seen in the single band in the 14-3-3η sample.

4.2 NUCLEAR MAGNETIC RESONANCE EXPERIMENTS

4.2.1 Analyzing the α-Synuclein fingerprint spectrum

In order to obtain a fingerprint of αS, a 2D ^{1}H^{15}N HSQC experiment was acquired on a 180μM ^{13}C^{15}N-labeled αS sample and processed in TopSpin (see Section 3.5 for details). The resulting HSQC spectrum of cross-peaks, correlating backbone and sidechain ^{15}N nuclei with ^{1}H nuclei through a single bond, thus provided a fingerprint of the αS protein (Figure 4.4). Due to the high number of detected cross-peaks (140), excluding false peaks (noise) and correlations likely representing side chains containing N-H bonds (Figure 4.4, circled), the spectrum of αS in pH 6.0 was deemed to be of satisfactory quality. This spectrum gave a representation of close to all 140 amino acids constituting monomeric αS, whereas αS in pH 6.8 and 7.4 resulted in lower sensitivities (see Supplementary Data for spectra overlay). By comparing chemical shifts with an existing αS assignment from BMRB (Entry 6968)[61], backbone residues were also assigned to cross-peaks with more distinct ^{1}H and/or ^{15}N δ values, displayed in Figure 4.4. Importantly, the fingerprint was used as an indication of the degree of folding; the peaks were more congregated rather than widely dispersed, with rather similar ^{1}H chemical shifts (Figure 4.4, ^{1}H

δ-axis). This further indicates a similar electron shielding environment for all residues, a phenomenon more often occurring when a protein is in an unfolded state.
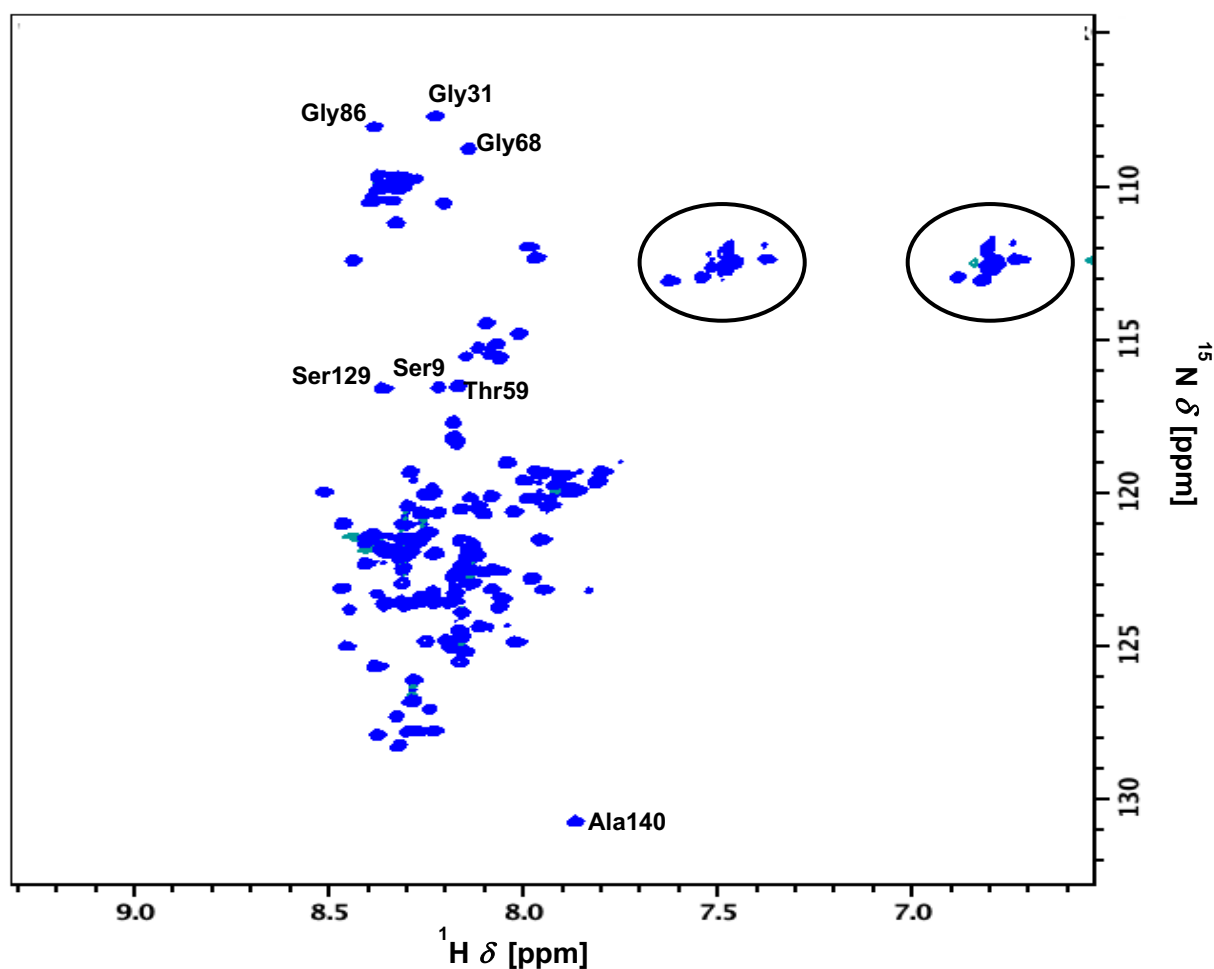
Figure 4.4 – 2D HSQC spectrum from $^{13}C^{15}N$ -labeled α-Synuclein (αS) at pH 6.0. The HSQC fingerprint of 180 μM ^{13}C ^{15}N-labeled monomeric αS detected 140 cross-peaks, representing the amino acid residues of the protein. Closely dispersed peaks along the F2 (^1H chemical shift, δ) and F1 (^{15}N chemical shift, δ) axis are indicates of an unfolded protein, corresponding to the intrinsically disordered native state of αS. Cross-peaks representing side-chain H–N correlations are circled. Data were collected at 25°C on the 850 MHz Bruker Advanced III HD Spectrometer.

4.2.2 Improving the fingerprint spectrum of 14-3-3η

Various NMR experiments were acquired on $^{13}C^{15}N$-labeled (double-labeled) and $^2H^{13}C^{15}N$-labeled (triple-labeled) 14-3-3η to obtain a fingerprint, and the resulting spectra were processed in TopSpin (see Section 3.5 for details). Firstly, a 2D $^1H^{15}N$ HSQC experiment was acquired on 264 μM double-labeled 14-3-3η, which after processing yielded the 2D HSQC spectrum presented in Figure 4.5. However, this labeling and experiment (see Table 3) produced a spectrum of poor quality despite the high protein concentration and purity of the sample. Compared to the total of 246 residues comprising 14-3-3η[50], very few cross-peaks were detected. Excluding the peaks that likely represented sidechains (Figure 4.5, circled), only 24 cross-peaks appeared in the HSQC spectrum – the fold could therefore not be evaluated based on this result, nor could a backbone assignment be performed. Given the considerable size and dimeric structure of 14-3-3η, further optimizations to the experimental procedure and acquisition parameters were required to obtain more sensitive signal detection for this protein.
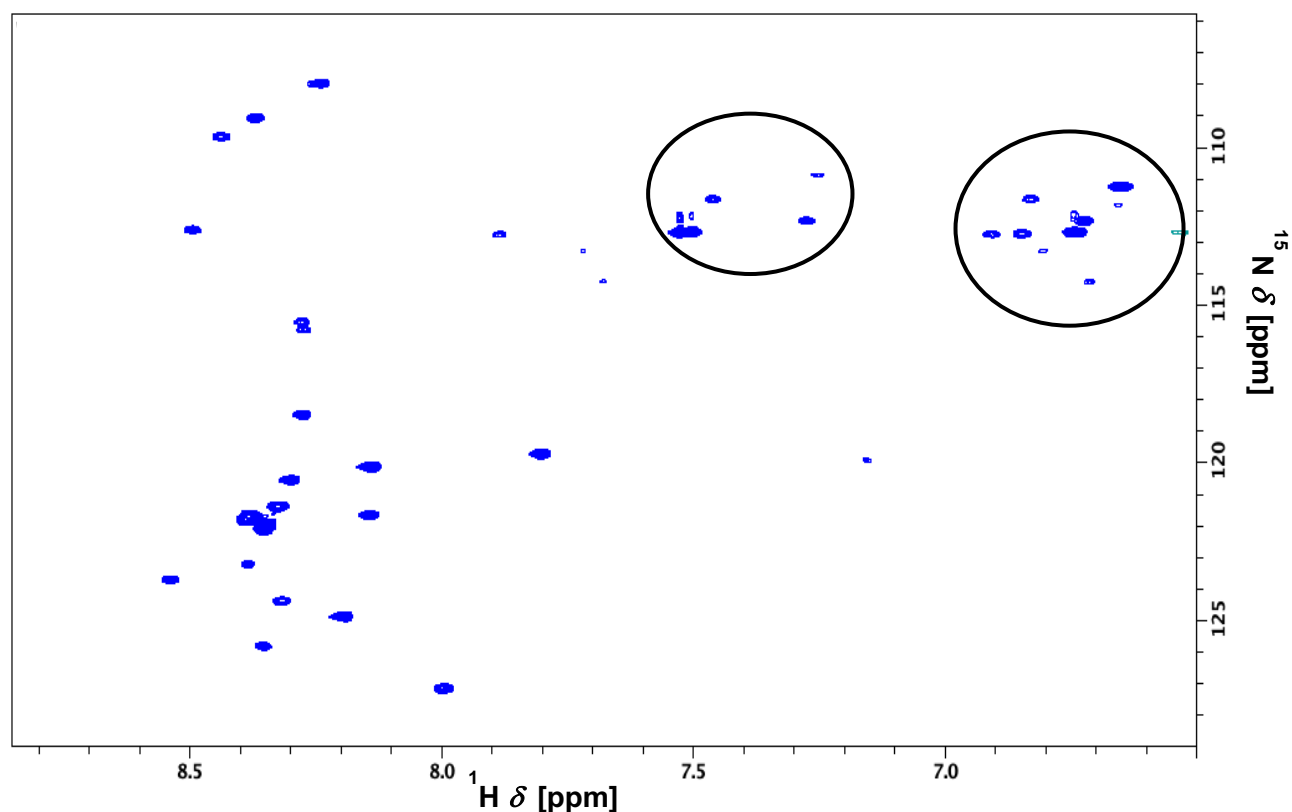
Figure 4.5 – 2D HSQC spectrum of $^{13}C^{15}N$-labeled 14-3-3η. $^1H^{15}N$ HSQC experiments (10 scans) were acquired on 264 μM $^{13}C^{15}N$-labeled 14-3-3η. Excluding sidechain correlations, this fingerprint spectrum detected 24 cross-peaks, representing 24/246 residues in 14-3-3η. Cross-peaks likely representing sidechain correlations are circled. Data were collected at 25°C on the 850 MHz Bruker Advanced III HD Spectrometer.

To improve the 14-3-3η fingerprint spectrum, we attempted to decrease the relaxation rates by labeling the protein with ^{2}H in addition to ^{13}C and ^{15}N (triple-labeled). Furthermore, a ^{1}H^{15}N TROSY-HSQC experiment was performed in addition to the standard ^{1}H^{15}N HSQC to compensate for the fast relaxation rates[58], and the number of scans increased to 224 scans per experiment (see Table 3). However, interruptions in the protein purification process caused the protein sample quality to decrease, yielding an estimated protein concentration of 50 μM triple-labeled 14-3-3η. Despite the lowered sample protein concentration, processed HSQC and TROSY-HSQC spectra still revealed an improved signal detection, presented as an overlay of spectra in Figure 4.6. Triple-labeling the protein and increasing the number of scans resulted in an HSCQ spectrum where 29 cross-peaks were detected (blue), excluding the sidechain correlations (circled). Applying TROSY-HSQC to the same sample did not lead to the detection of sidechain correlations, but further increased the sensitivity for backbone signals; 36 cross-peaks appeared in the TROSY-HSQC spectrum (green), though slightly shifting the peaks. Moreover, the detection of these additional residues allowed for an estimation of the protein fold. The wider dispersion of cross-peaks along the ^{1}H δ axis in Figure 4.6 suggests a larger variation in nuclei chemical environments, corresponding to the spectrum of a folded protein. However, the improved TROSY-HSQC spectrum obtained in this study did not detect a sufficient number of cross-peaks to perform a 14-3-3η backbone assignment required for interaction studies.
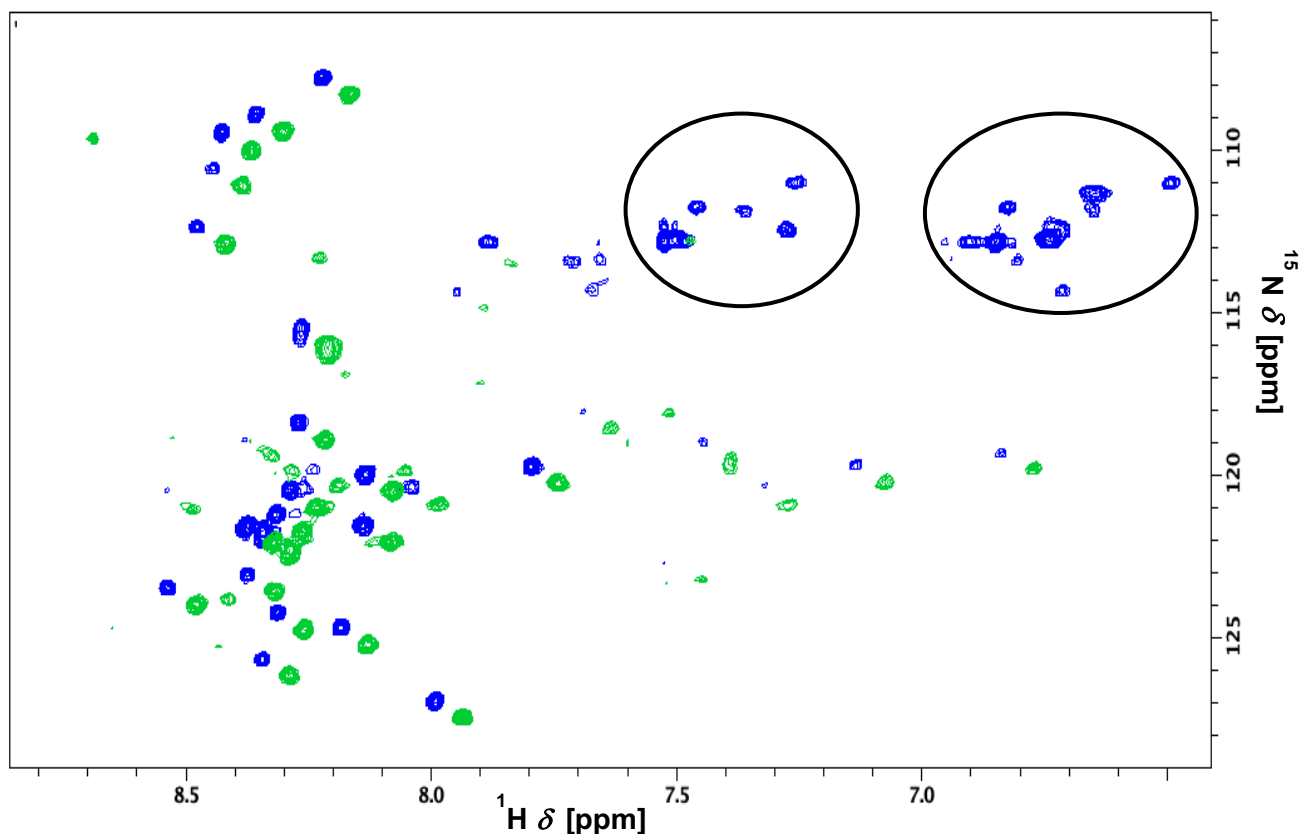
Figure 4.6 – ***Overlay of 2D HSQC and 2D TROSY-HSQC spectra of $^2H^{13}C^{15}N$-labeled 14-3-3η.*** $^1H^{15}N$ HSQC and TROSY-HSQC experiments (224 scans) were acquired on 50 μM $^2H^{13}C^{15}N$-labeled 14-3-3η and processed in TopSpin 4.0.7. The HSQC spectra (blue) detected 29 cross-peaks representing backbone correlations, as well as certain sidechain correlations (circled). The TROSY-HSQC spectrum detected seven additional peaks, improving the sensitivity and removing the side chain correlations. The less closely dispersed cross-peaks indicates a folded protein structure. Data were collected at 25°C on the 850 MHz Bruker Advanced III HD Spectrometer.

4.3 ThT-MONITORED α-SYNUCLEIN AGGREGATION ASSAYS

Under the conditions of shaking and a temperature of 37°C, αS can self-associate and form fibrillar aggregates *in vitro*[54]. However, there are indications that the 14-3-3η isoform could affect the kinetics of this process by suppressing fibril formation[9] (see Section 1.7.2). To study the effects of 14-3-3η on αS aggregation, ThT-monitored aggregation assays were performed with αS in the presence of 14-3-3η (see Section 3.6.2 for details). Due to the β-sheet dependent fluorescence of ThT, the resulting fluorescence signals could be used as a measure of the degree of αS fibrillation.

4.3.1 Analysis of α-Synuclein fibrillation curves

Aggregation assays of αS and 14-3-3η yielded one fibrillation curve per sample well, showing the ThT fluorescence intensity over time for each well in a sample (see Section 3.6.2). After data accumulation, the raw fluorescence data obtained with FLUOStar Optima Microplate Fluorescence Reader was processed with MatLab. Two of the replicates did not yield applicable results, as no fibrillation was observed for the αS positive controls. Only one replicate was therefore obtained for the BSA and FA-free BSA control samples within the time-restrictions of the project. Typical examples of fibrillation curves are displayed in Figure 4.7 a-d, which shows an apparent difference in αS fibrillation between the absence (a) and presence (b-d) of 14-3-3η. On initial observation of the fibrillation curves alone, the fluorescence signal in 100 μM αS appeared to increase early on and with steep slopes in all replicates (see Supplementary data for all fibrillation curves). Addition of 10, 20 and 55μM 14-3-3η seemingly caused a notable delay in the starting points and a decrease in the slope of the curves, indicating an attenuating effect on αS aggregation. However, further processing in the form of model fitting, parameter extraction and statistical analysis was required to confirm initial observations. Fitting of individual curves and extraction of aggregation parameters were therefore performed based on these fibrillation curves.

Figure 4.7 – ThT-monitored α-Synuclein (αS) fibrillation curves in the absence and presence of 14-3-3η.
The aggregation of αS was monitored by the fibril-dependent fluorescence of ThT, creating a fluorescent signal increasing with fibril growth. Samples were prepared with 100 μM αS and 5 μM ThT in each sample, and 10-55 μM of 14-3-3η, with 15 wells/sample. Data were collected with FLUOStar Optima Microplate Fluorescence Reader. The selection of fibrillation curves shows the development of ThT fluorescence and thus fibrillation in a) 100 μM αS, b) αS + 10 μM 14-3-3η, c) αS + 20 μM 14-3-3η, and d) αS + 55 μM 14-3-3η. Fibrillation appeared to decrease by the addition of 14-3-3η, seen in the increasing difference from a) to d).

4.3.2 Extraction of kinetic parameters from the two-step aggregation model

From the characteristic sigmoidal growth profile of typical αS aggregation and fibril growth, two kinetic parameters were extracted; the fibrillation constant, v, describing the rate of fibrillation (the slope), and the lag time, t_n, describing the time until fibrillation occurs (see Section 3.6.2). After processing of the fluorescence signals, individual fibrillation curves of all wells from each sample were processed by normalizing the fluorescence signal and fitting the data to a two-step model (Section 3.6.2, Equation 1 and 2). This resulted in a sigmoidal fit, an example of which is displayed in Figure 4.8, a (red). Hence, v and t_n could be extracted directly from the fits for all samples with fits of satisfactory quality ($r^2 > 0.95$). However, this fit proved

unattainable for some of the curves in question (example in Figure 4.8, b), e.g. from wells in which the fluorescence signals remained approximately the same throughout the assay. Consequently, the number of successful fits differed from the total amount (Table 4).
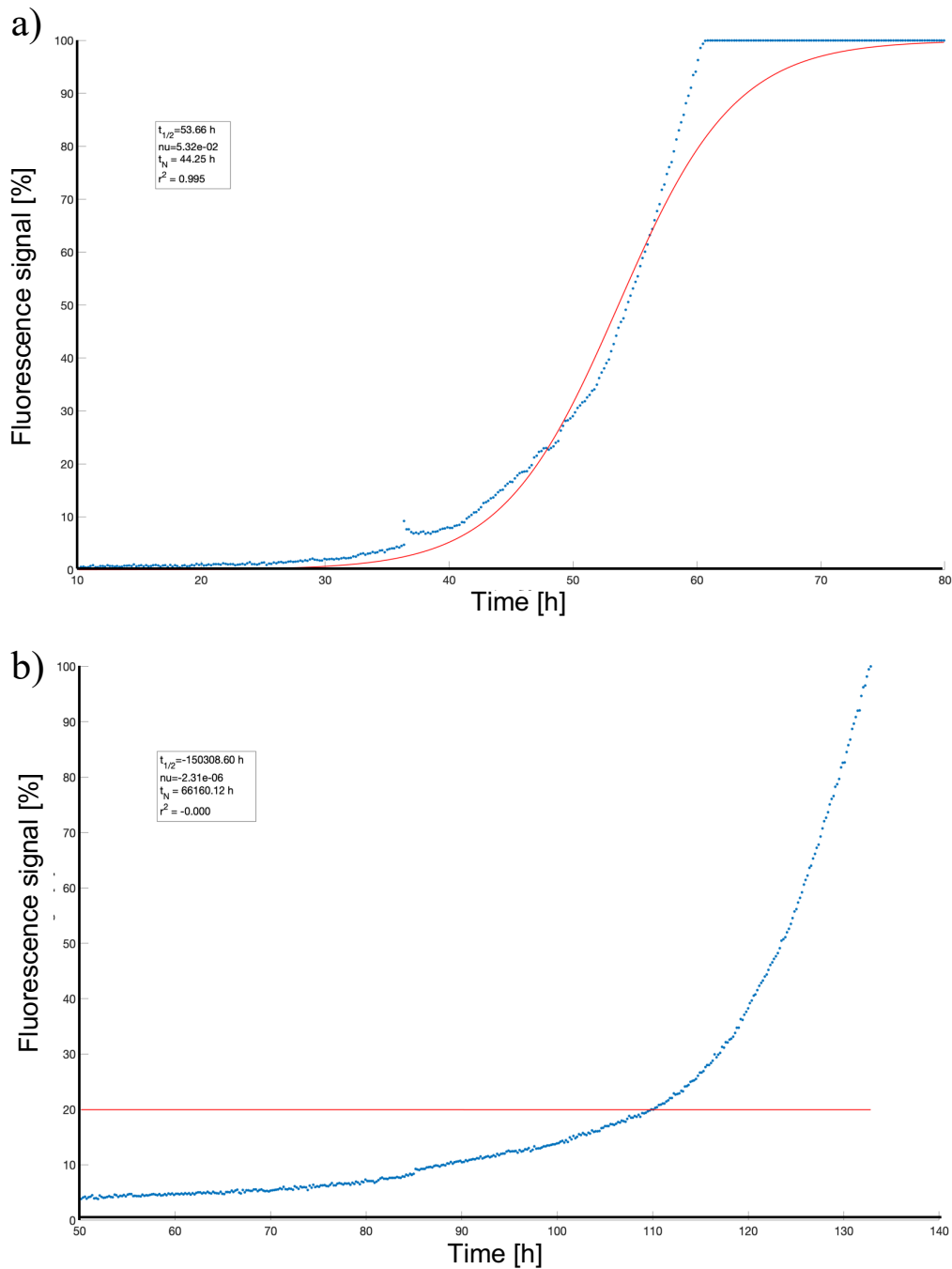
Figure 4.8 – Normalized single fibrillation curves fitted to the two-step aggregation model. Fibrillation curves from samples containing αS and 14-3-3η were fitted to a sigmoidal model representing the aggregation of αS, to extract the rate constant ν and the lag time t_n. The quality of the fits was evaluated based on their r^2-value, and fits with $r^2 > 0.95$ were deemed satisfactory. Displayed are examples of a high quality fit in a sample of 100 μM αS, yielding a sigmoidal fit and an $r^2 = 0.995$ of the fitted curve (a, red line), and an example of curve which fitted poorly to the data, as seen by the horizontal fit line (red) and the negative r^2 value close to zero (b).

Table 4: Proportion of successful fits in each sample type

Sample	Successful fits/Total amount of fits
100 µM αS	42/45
αS + 55 µM BSA	5/15
αS + 55 µM FA-free BSA	15/15
αS + 10 µM 14-3-3η	25/45
αS + 20 µM 14-3-3η	25/45
αS + 55 µM 14-3-3η	21/45

4.3.3 The effects of 14-3-3η on the lag time of α-Synuclein fibrillation

To assess the changes in fibrillation rates and/or lag times, the mean values of extracted parameters ν and t_n for each sample were normalized to the positive control (100 µM αS), to assess whether any change in fibrillation rates and/or lag times occurred. On initial comparison of the different mean t_n values, the most prominent effect was seen for the addition of 20 µm 14-3-3η. This caused an apparent 139% increase in fibrillation lag time compared to the αS control. Similarly, 10 µM 14-3-3η caused an apparent 121% increase, while 55 µM 14-3-3η increased the lag time by 66% compared to the control (Figure 4.9). These observations suggest that 14-3-3η indeed slows the onset of αS fibrillation and that this effect could be dose dependent. However, statistical analysis revealed no significant differences in lag times between the αS control and αS supplemented with 14-3-3η, nor between the different dosages of 14-3-3η (Welch t-tests; n=3; $P > 0.05$, see Supplementary data for all statistical parameters). Nevertheless, the observed difference, though not significant in this study, was deemed noteworthy and possibly interesting for further studies with a greater number of replicates. While the control samples with BSA and FA-free BSA were more similar to the αS positive control, these results were considered inconclusive, given that only one replicate was obtained, and no statistical analysis could be performed.
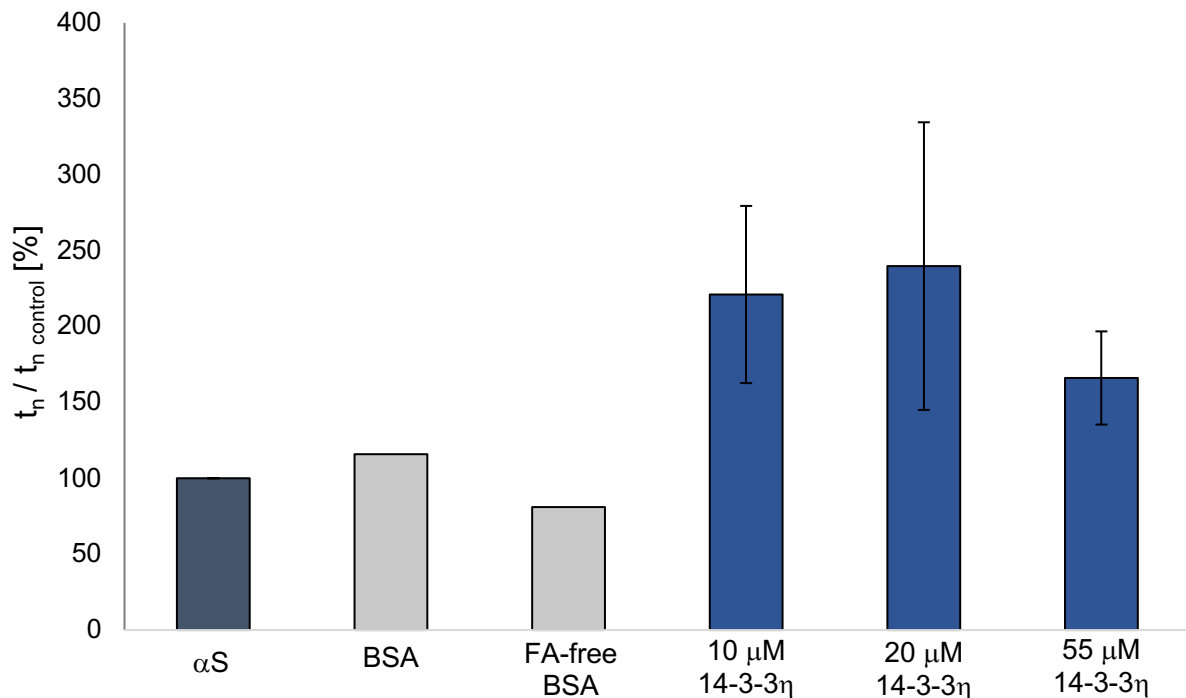
Figure 4.9 – The effect of 14-3-3η on the lag times of α-Synuclein (αS) fibrillation. Normalized mean lag times, t_n, of αS fibrillation from the different samples were extracted from model fits based on fibril-dependent ThT-fluorescence. 100 μM αS was present in all samples. Mean t_n values for each sample were normalized with respect to the αS positive control. Despite the apparent increase in lag time as a result of 14-3-3η, no statistically significant differences were detected between any of the samples (Welch t-tests; n=3; $P > 0.05$).

4.3.4 The effects of 14-3-3η on the rate of α-Synuclein fibrillation

Regarding the rates of αS fibrillation, the results immediately revealed a change resulting from the presence of 14-3-3η. Upon observation of the normalized mean v values (Figure 4.10), the fibrillation rates decreased by more than 50% from the αS control in samples containing14-3-3η, suggesting that the presence of 14-3-3η slows the rate of αS fibrillation. Moreover, statistical analysis showed that 14-3-3η in concentrations of 10 and 55 μM significantly decreased the rate of αS fibrillation by 58 and 68% compared to αS control, respectively (Welch t-test; n=3; $P < 0.05$*, see Supplementary data). Furthermore, there were no significant differences between the effects observed by addition of 10 and 55 μM 14-3-3η, indicating that an increase in the 14-3-3η dosage is not necessarily proportional to the decrease in fibrillation rate (Welch t-test; n=3; $P > 0.05$). 20 μM 14-3-3η did not yield a significant decrease from the αS control sample (Welch t-test; n=3; $P > 0.05$). Nevertheless, this could be due to the high

standard deviation and variance in the ν values rather than that there was no actual influence, implying that further studies are necessary to achieve a conclusive result. Interestingly, BSA appeared to have the greatest effect on the αS fibrillation rate, decreasing the rate by 87%, whereas the addition of FA-free BSA did not seem to lower the rate to any great extent. Although this could be an indication of the fatty acids in the BSA interacting with αS and lowering the fibrillation rate, one replicate was not enough to perform statistical analysis, as previously mentioned. Results with BSA and FA-free BSA were therefore deemed inconclusive. Hence, results with 14-3-3η could not be compared to any control samples in these assays with full confidence.
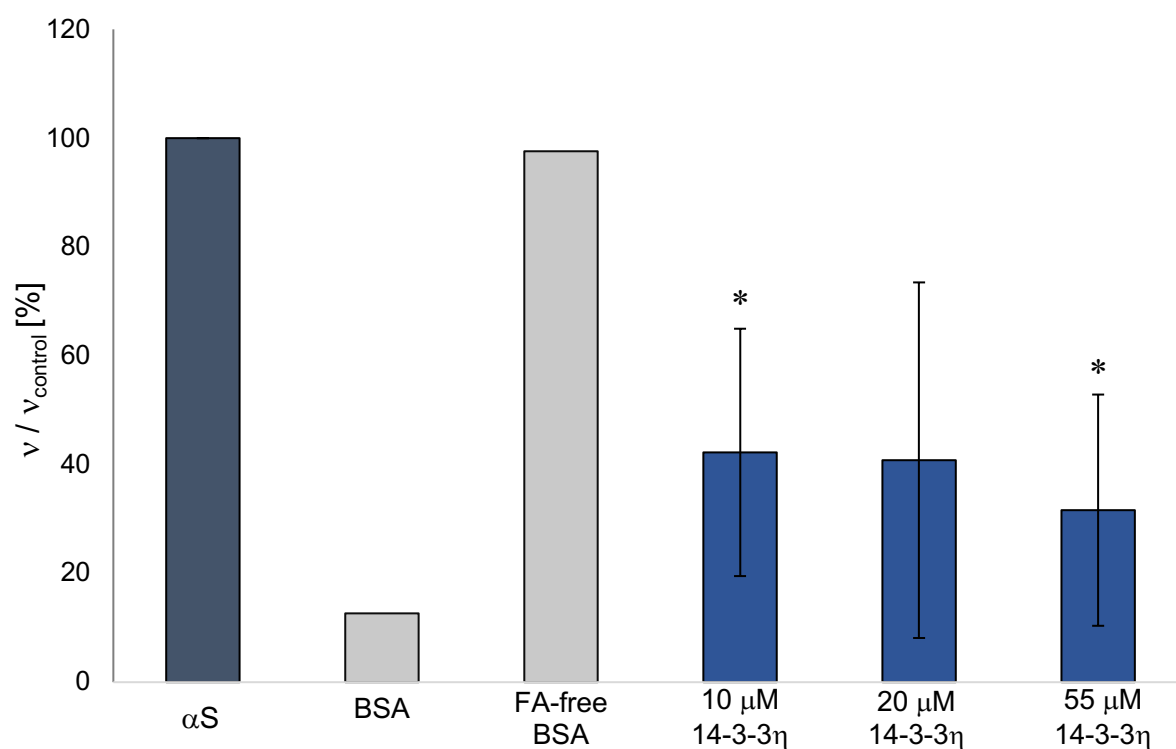
Figure 4.10 – The effect of 14-3-3η on α-Synuclein (αS) fibrillation rates. The normalized mean fibrillation rates, ν, of αS aggregation from the different samples were extracted from model fits based on fibril-dependent ThT-fluorescence. 100 μM αS was present in all samples. 10 and 20 μM 14-3-3η significantly decreased the αS fibrillation rates compared to the αS positive control (Welch t-tests; n=3; $P < 0.05*$). The suppressing effects of 14-3-3η on αS fibrillation rates did not prove to be dose dependent (Welch t-tests; n=3; $P > 0.05$).

4.3.5 Cumulative analysis of α-Synuclein aggregation and the effects of 14-3-3η

In addition to the fibrillation curves and kinetic parameters, the wells from each replicate were analyzed using an approach that is able to handle the stochastic nature of αS aggregation onset and propagation[54] (see Section 3.6.2). This analysis is based on tracking the cumulative number of positive wells in each sample for each experimental replicate. To find the total percentage of aggregation-positive wells per sample, a threshold of a fluorescence signal three-fold higher than the maximum noise was used.

In addition to providing an overview of the total effects of 14-3-3η in different doses, this representation also highlighted the variation between the three replicates (Figure 4.11 a-c). In samples containing 14-3-3η, the total percentage of wells after ~140 hours ranged from 30-100%, depending on the replicate. Nevertheless, notable differences were observed from the αS control samples. Whereas uninhibited αS increased in positive wells from 20-25 hours and rapidly reached 100%, αS containing 14-3-3η displayed no positive wells until 50-60 hours had passed. The transition from 0 to 100% also progressed at a slower pace in the 14-3-3η samples, altogether indicating that 14-3-3η could slow the total aggregation process of αS. We provided further statistical support for this assumption by obtaining the average percentage of positive wells (APPW) in each sample over time and normalizing it to the αS control (see Supplementary data). We found that 14-3-3η significantly decreased the APPW over time (Welch t-tests; n = 3; $P < 0.05^*$), suggesting that 14-3-3η attenuates the overall αS fibrillation process. 55 μM 14-3-3η had the most prominent effect on aggregation, producing a 0.9-fold decrease in APPW from the αS control (Welch t-test; n = 3; $P < 0.01^{**}$).

In correspondence with the lowered rate of fibrillation resulting from BSA (Figure 4.10), the percentage of positive wells was also clearly affected by BSA (Figure 4.11, b), with < 20% aggregation positive wells. The striking difference between BSA and FA-free BSA also became clear in this representation, as the addition of FA-free BSA produced a curve nearly identical to the positive αS control (Figure 4.11, c). Moreover, FA-free BSA did not affect αS aggregation, while BSA yielded close to a 1-fold decrease in the APPW (see Supplementary data).
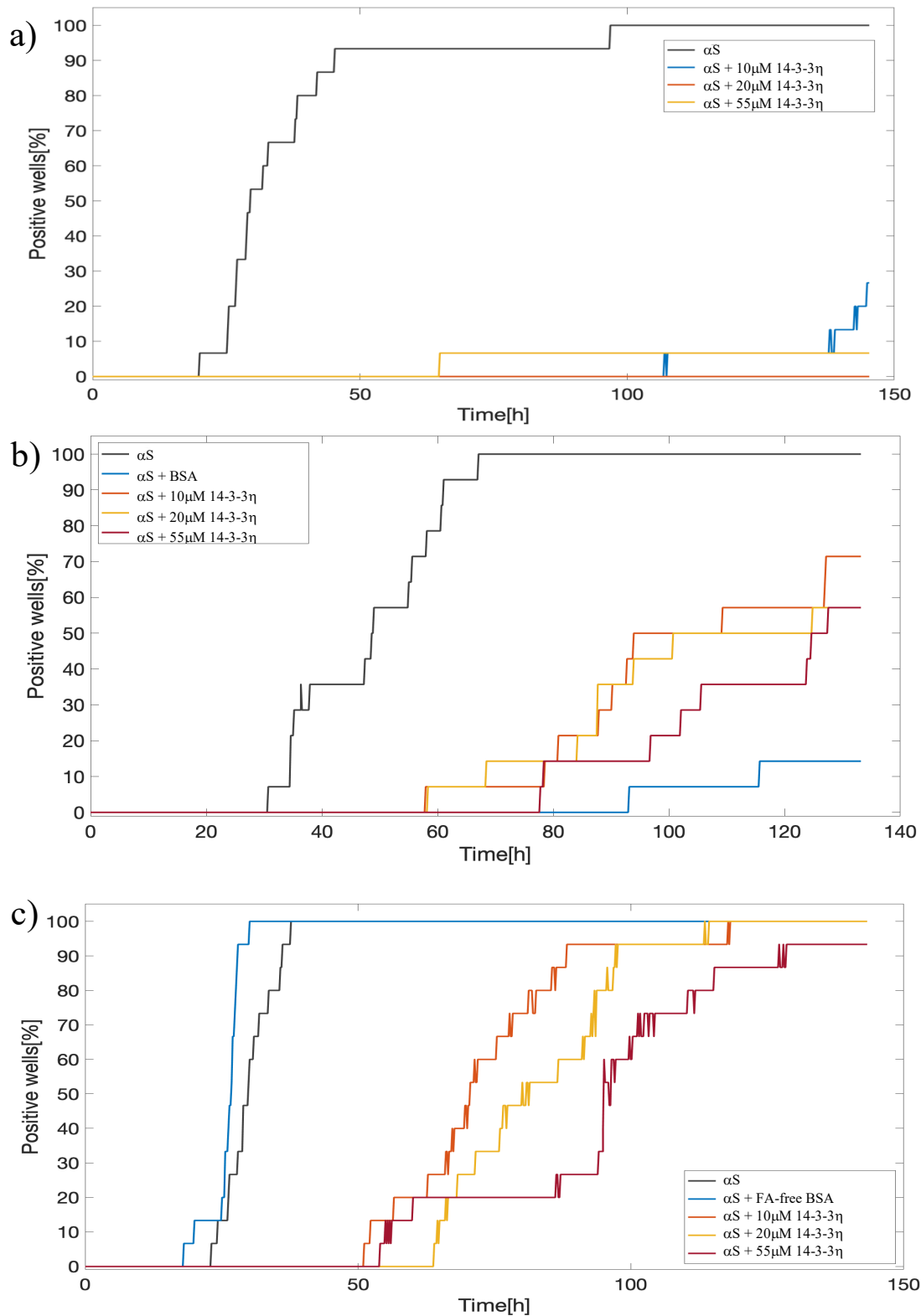
Figure 4.11 – Cumulative representation of α-Synuclein (αS) aggregation positive wells and the effects of 14-3-3η. αS aggregation were monitored by the fibril-dependent fluorescence of ThT, creating a fluorescent signal increasing with fibril growth. Cumulative analysis of each of the three experiment replicates was performed to find the percentage of aggregation positive wells/sample, i.e. where the fluorescent signal ascended three-fold of the noise. Panel a) – c) displays results from the first, second and third replicate, respectively. The percentage of positive wells was observed to decline in samples containing 14-3-3η for all replicates.

4.4 SURFACE PLASMON RESONANCE INTERACTION STUDIES

There are several indications that 14-3-3η interacts with αS in the parkinsonian brain (Section 1.7.2), and our results from aggregation assays (Section 4.3) implied that this interaction could attenuate the aggregation of αS. However, the properties of this interaction have yet to be fully described. SPR was utilized to characterize the binding of 14-3-3η to monomeric αS. The interaction between 14-3-3η in solution and monomeric αS immobilized on a CM5 sensor chip was reported in arbitrary response units (RU) to determine the affinity of binding (see Section 3.7). HBS-EP+ buffer was injected onto the chip to control the occurrence of non-specific binding. The response (RU) upon each injection was detected to evaluate whether binding occurred. Injections of the buffer control yielded no response, indicating no non-specific binding to the chip. All buffer injections yielded RU equal to or below zero (Figure 4.12). Regarding the binding between 14-3-3η and the monomeric αS, negative values of approximately -15 RU were detected as a response to the injections of 0.5-1.0 μM, indicating that no binding had occurred (Figure 4.12). Increasing 14-3-3η concentrations to 2.5-10 μM yielded little increase in the detected response, with 0.55 RU for 10 μM 14-3-3η. Hence, the response and difference from 14-3-3η to the buffer control was deemed dismissible, suggesting that 14-3-3η was not able to bind monomeric αS. However, only one experiment was performed, leaving statistical analysis infeasible.
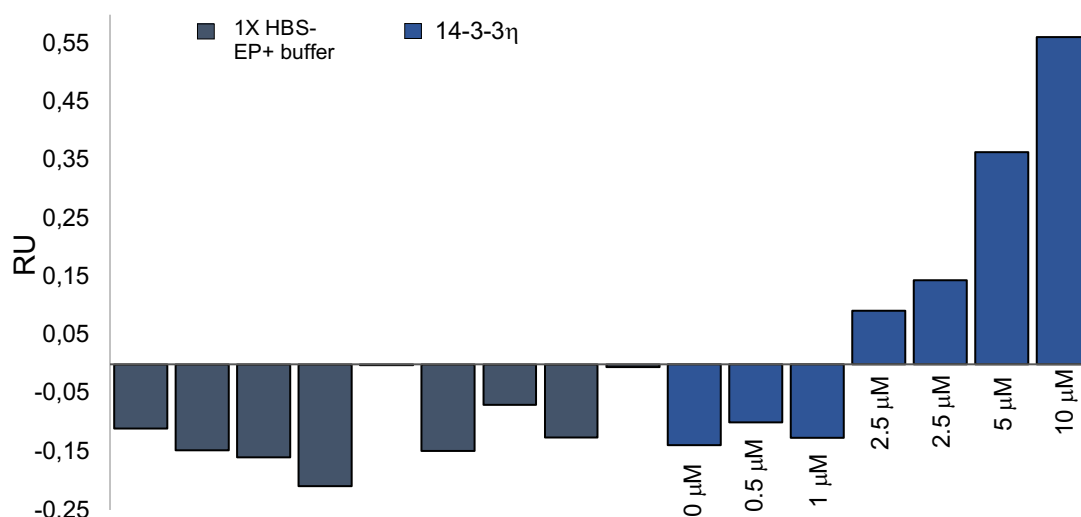
Figure 4.12 – Interaction between 14-3-3η and α-Synuclein analyzed by SPR. 14-3-3η in concentrations of 0.5-10 μM were injected onto 1900 RU of monomeric αS immobilized to a CM5 sensor chip and the reference cell. Binding analysis was performed on the BiaCore T200 with flow rate 25 μl/min, 240 s contact time, 600s dissociation time, 30 s stabilization period and the chip was regenerated with 10 mM Glycine pH 2.2 at 30 μl/min between each concentration. The recorded RU indicated no binding of 14-3-3η to monomeric αS.

5. DISCUSSION

Fibrillar αS aggregates have been discovered to be the primary component of LBs, insoluble neuronal inclusions characteristic of Parkinsonian brains. The misfolding and aggregation of αS, preceding the formation of LBs, is thus considered central to PD[6]. However, it remains enigmatic why this intrinsically disordered protein misfolds and aggregates, and how to prevent it. In this context, the 14-3-3 family of scaffold proteins with chaperone-like activities have come of interest as possible suppressors of αS aggregation[47]. In particular, the 14-3-3η isoform was discovered to interact with αS in a way that attenuates and reroutes its fibrillation, and has been co-immunoprecipitated with αS from Parkinsonian brains[9,52]. In this study, we aimed to elucidate upon the effects of 14-3-3η on the kinetics of αS aggregation *in vitro,* employing ThT aggregation assays and subsequent evaluation of fibrillation curves. We further attempted to characterize the binding properties of the two proteins utilizing NMR and SPR.

5.1 α-SYNUCLEIN AND 14-3-3η NMR SAMPLES INDICATE POTENTIAL FOR FURTHER CHARACTERIZATION

The success of NMR spectroscopy relies on several factors. Firstly, the sample quality affects the quality of the spectra as well. A sufficient protein concentration, optimal buffer conditions and the correct isotope labeling scheme are all required in a high-quality sample[62]. Moreover, intrinsic protein properties such as size and conformation affect the resolution and sensitivity of an NMR experiment[57]. In this study, NMR spectroscopy was employed to obtain HSQC fingerprints and verify the protein fold of αS and 14-3-3η. Such HSQC experiments are generally the first step and a prerequisite for proceeding with analysis in protein NMR[62]. Moreover, it was attempted to obtain a 14-3-3η fingerprint spectrum satisfactory for backbone resonance assignment to be used in future NMR interaction studies.

5.1.1 HSQC fingerprint of α-Synuclein confirms its disordered state

HSQC experiments on uniformly 180 μM $^{13}C^{15}N$-labeled αS resulted in a high-quality fingerprint spectrum with all 140 residues represented (Figure 4.4), with the exception of prolines, in addition to side chains containing the N-H amine bond. Because residues in an unfolded protein will experience rather similar chemical environments, their chemical shifts will be similar as well. This will in turn produce a spectrum where the cross-peaks are not as dispersed as for a folded protein with a tertiary structure. The αS HSQC spectrum with closely dispersed cross-peaks therefore indicates that the protein is indeed unfolded, as expected from

the intrinsically disordered state of monomeric αS. Used as a quality assessment for products of the αS expression system, this supports that the expression system does yield monomers in solution. Moreover, the chemical shifts of the cross-peaks could be used to complete an αS backbone assignment if triple-resonance experiments are acquired. This would allow for more accurate assignment, as triple-resonance experiments enable better cross-peak dispersion, sequential connectivity between amino acid residues and better differentiation between amino acid type based on the ^{13}C chemical shift. However, the time restrictions of this project did not allow for such experiments, and the current partial assignment is based only on ^{1}H and ^{15} chemical shifts and an existing assignment by Bermel *et al*[61].

5.1.2 ^{2}H-labeling and TROSY-HSQC improves the sensitivity of 14-3-3η signal detection

The ^{1}H^{15}N HSQC experiments acquired on ^{13}C^{15}N-labeled (double-labeled) 264 μM 14-3-3η yielded a fingerprint spectrum of poor quality, with only 24/246 backbone residues detected (Figure 4.5). As such, the fold could not be evaluated from the insufficient number of cross-peaks. This low sensitivity can be attributed to the size of 14-3-3η. While ^{13}C^{15}N -labeling and 10 scans per experiment proved sufficient to detect the αS backbone signals, the 28 kDa 14-3-3η is a considerably larger protein, comprising 246 residues[50]. For large proteins, a high number of ^{1}H nuclei and slow tumbling makes dipole-dipole relaxation pathways more efficient than for smaller proteins. As a result, the relaxation rates increase, which in turn causes signal broadening to the point where individual residues are difficult to detect (Section 1.8.2)[57]. Moreover, 14-3-3η's dimeric state likely posed another challenge for this type of experiment, as the monomer-dimer equilibrium may reduce spectral quality[63].

To combat the issues of protein size, 14-3-3η was expressed with ^{2}H in addition to ^{13}C and ^{15}N (triple-labeling) to interfere with the ^{1}H nuclei interactions, yielding a sample of ~50 μM 14-3-3η. This has the effect of thinning out the ^{1}H nuclei responsible for the efficient relaxation[57]. Furthermore, the number of scans was increased to 224 scans per experiment (Table 3) and ^{1}H^{15}N TROSY-HSQC was employed to compensate for the fast relaxation rates[58]. With these methodological optimizations, we were able to get fingerprint spectra with 29/246 and 36/246 residues represented in the HSQC and TROSY-HSQC spectra, respectively (Figure 4.6). Although this is a relative improvement from the HSQC of the double-labeled sample, the TROSY-HSQC spectrum quality remained too poor to extend the data accumulation to triple-resonance experiments for backbone assignment. However, we suggest that this is attributed to

the low protein concentration in the sample, which lowers the sample quality, rather than the experimental approach.

Regardless, we propose that triple-labeling and TROSY-HSQC experiments described in this study can be employed to achieve a satisfactory fingerprint spectrum of 14-3-3η if a more concentrated triple-labeled sample is prepared. Indeed, a similar approach was utilized in a study of 14-3-3ζ by Killoran *et al*[64], who performed a 14-3-3ζ assignment (BMRB: 25231) and binding studies based on the $^1H^{15}N$ TROSY-HSQC spectrum. Using this assignment as a reference, a proper 14-3-3η fingerprint spectrum could provide a partial backbone assignment also for 14-3-3η, although each assignment should be verified using the appropriate triple-resonance techniques, namely HNCA, HNCACB, HNCOCACB. A complete assignment could then be used to identify residues involved in αS binding by titrating with unlabeled αS, then identifying the residue-specific changes in the 14-3-3η fingerprint.

5.2 14-3-3η AFFECTS THE KINETICS OF α-SYNUCLEIN FIBRILLATION

Previous studies have implicated 14-3-3η as an interaction partner and influencing factor of αS aggregation (see Section 1.7). To study whether 14-3-3η affects the kinetics of αS fibrillation, we utilized ThT-monitored aggregation assays with αS in the absence and presence of 14-3-3η. Fluorescence curves processed from raw experimental data revealed a clear tendency of decreased fibrillation onset and rate as a result of 14-3-3η (Figure 4.7 and Supplementary data). However, no conclusions could be drawn from these curves alone, as the stochastic nature of fibrillation caused each replicate to differ considerably. The data was therefore fitted to a two-step model (Section 3.6.2) to obtain kinetic parameters and form the basis for a more tangible approach to data evaluation.

5.2.1 Preliminary curve fitting data suggests 14-3-3η may suppress fibrillation

Fitting the normalized fluorescence curves to a two-step model (Section 3.6.2) provided curve fits from which kinetic parameters t_n (lag time) and v (fibrillation rate constant) could be extracted. Although several fits proved not successful for parameter extraction, this alone could indicate attenuating effects of 14-3-3η. When comparing the proportion of high-quality fits in the αS control samples and samples containing 14-3-3η (Table 4), unperturbed αS aggregation gives fluorescence data that fit well to the sigmoidal model and thus a large proportion of successful fits. Conversely, the presence of 14-3-3η appears to give data less suitable for the

sigmoidal fit, and a flattened curve. This suggests that 14-3-3η in some cases may have greatly impeded fibrillation onset, i.e. that the lag time exceeded the assay time, or even that 14-3-3η suppressed fibrillation completely. This observation is further supported by Plotegher et al[9], who found that the presence of 14-3-3η with αS caused a negligible increase in ThT fluorescence, and thus αS fibrillation. As such, extending the assay time could be beneficial to obtain a higher proportion of successful fits and thus a complete set of parameters from each replicate.

5.2.2 14-3-3η Significantly attenuates fibrillation growth rates and overall fibrillation

The extraction of kinetic parameters from the fitted curves enabled a more precise assessment of the experimental data. Preliminary comparisons of mean t_n (lag times) normalized to the αS control indicated that 14-3-3η could increase the fibrillation lag time by up to 139% (Figure 4.9), thus attenuating fibrillation onset. However, the effects of 14-3-3η on αS fibrillation lag time were not attenuating to a significant degree (Welch t-tests; n=3; $P > 0.05$), suggesting that 14-3-3η does not interfere with αS fibrillation onset. Regardless, this non-significance could be due to an insufficient number of replicates in combination with the great variations between them. Given the large apparent effects observed in this study, 14-3-3η might have significantly prolonged the αS fibrillation lag time if the number of replicates and the assay time were increased to minimize statistical variations.

Although 14-3-3η induced no significant changes in αS fibrillation onset, it significantly decreased the αS fibrillation rate (Welch t-tests; n=3, $P < 0.05*$, Figure 4.10), indicating that 14-3-3η interferes with secondary nucleation in the fibrillation process (see Section 1.4). Evaluation of mean fibrillation rates, v, normalized to the αS control revealed that 55 μM 14-3-3η decreases the fibrillation rate by 68%. Interestingly, 10 μM 14-3-3η induced a similar drop in the fibrillation rate (58%), so the attenuating effects were not dose-dependent (Welch t-test; n = 3, $P > 0.05$). These results imply that 14-3-3η can significantly slow αS fibril growth even in αS:14-3-3η ratios of 10:1. As a ratio of 2:1 does not further decrease the growth rate, 14-3-3η could have reached a saturation point as suggested by Plotegher et al[9]. However, it is also possible that the concentrations used in this study were too similar to yield any dose-dependency. Performing additional experiments with 1:1, 1:2 and higher ratios would be needed to confirm these observations. Experiments with ratios of 15:1, 20:1 and lower would also be beneficial to explore the threshold at which 14-3-3η becomes attenuating.

Additionally, cumulative aggregation analysis of individual replicates showed the percentage of aggregation positive wells to remain 0% for an extended time in wells containing 14-3-3η compared to those containing αS alone (Figure 4.11). 14-3-3η was shown to significantly decrease the overall aggregation, represented by the APPW, for all ratios used in this study (Welch t-tests; n = 3, $P < 0.05$*, see Supplementary data), with the most prominent effect on APPW observed for 55 μM 14-3-3η (Welch t-test; n = 3; $P < 0.01$**). No significant differences were detected between the different 14-3-3η concentrations (Welch t-tests; n = 3; $P > 0.5$), further supporting that the attenuation by 14-3-3η is not dose-dependent. As this type of analysis takes the complete dataset into account, we obtained a more robust, though less specific, significance in the results as well. Furthermore, the variations between the replicates become clear in the high standard deviations (Figure 4.10) for each sample and the cumulative aggregation analysis of each replicate (Figure 4.11). This variation could be an explanation for why 20 μm 14-3-3η yielded no significant effect on αS fibril growth rates (Welch t-test; n = 3, $P > 0.05$). Because this concentration lies in the range between 10 and 55 μM, it is likely that this non-significant result was due to an insufficient number of replicates and large variances, similar to the t_n results. We therefore propose that 14-3-3η attenuates the overall aggregation process through decreasing the fibril growth rate, and likely the fibrillation onset as well.

In addition to samples with αS and 14-3-3η, BSA and FA-free BSA were added to αS to assess whether the attenuating effects were due to 14-3-3η or the addition of any protein in itself. The size of BSA (66 kDa) is roughly similar to the 14-3-3η dimer (56 kDa), with approximately the same pI of 4.7-5.0. Although only one replicate was obtained for each of these samples, the results demonstrated a clear difference in their effects on αS aggregation. While FA-free BSA produced lag times and fibrillation rates (Figure 4.9, Figure 4.10) similar to αS alone, BSA containing fatty acids decreased the fibrillation rate by 87% (Figure 4.10). The difference also becomes highlighted in the cumulative aggregation analysis; the addition of BSA caused a negligible percentage of aggregation positive wells, and FA-free BSA produced a curve similar to the αS control (Figure 4.11, b-c). These results are likely attributed to the FAs in BSA interacting with αS (see Section 1.5.1), and that this interaction has a great influence on its fibrillation. Hence, FA chains in solution could be a suppressing factor in αS aggregation, despite that short FA chains in the membrane have been suggested as strong aggregation inducers[28], indicating that the organization of FAs is important for their influence on αS

aggregation. Moreover, the negligible effect of FA-free BSA suggests that 14-3-3η indeed causes the attenuation observed in this study. However, as one replicate does not yield any conclusive results nor statistical analysis, this cannot be stated with full confidence. Summarized, our results imply a role of 14-3-3η as an attenuating factor in αS fibrillation. However, ThT does not produce fluorescence signals until binding to β-sheets in the protofilaments and fibrils occur[54]. Therefore, these assays provide no information as to which αS aggregation stage 14-3-3η binds, or if it affects the oligomerization process. Using the 14-3-3η NMR results obtained in this study (See Section 4.2.2 and 5.1.2) however, we are well positioned to expand our knowledge on this matter in the future.

5.3 14-3-3η DOES NOT APPEAR TO BIND MONOMERIC α-SYNUCLEIN

In addition to the effects of 14-3-3η on αS aggregation observed in this study, studies with 14-3-3η and αS suggest that the two proteins interact[9,52]. To gain a more detailed understanding of this interaction, 14-3-3η and monomeric αS was investigated by SPR (see Section 3.7) to obtain accurate detection of a possible binding. Results from SPR binding analysis with 0.5-10 µM 14-3-3η revealed no binding response (Figure 4.12), suggesting that 14-3-3η is unable to bind monomeric αS. Although only one replicate was obtained due to time restrictions of the project, this suggestion is supported by native PAGE analysis and NMR studies of αS and 14-3-3η from Plotegher et al[9]. This study found that monomeric αS with 14-3-3η migrated as two distinct bands on a native PAGE, and that 14-3-3η did not affect the chemical shifts of monomeric αS, both indicative of no binding. However, their NMR approach could be improved, e.g. by analyzing peak volumes in addition to the configuration of the fingerprint. They further concluded with 14-3-3η being able to bind only to the oligomeric species of αS[9]. However, SPR studies by Sato et al[52] demonstrated an interaction between 14-3-3η and αS monomers with a binding affinity $K_d = 1.1$ µM, although this result could be caused by oligomer contaminations in the interaction. The results in this study therefore support the assumption by Plotegher et al[9] that 14-3-3η binds to oligomeric states of αS aggregation. This further implies that the interaction cannot affect αS oligomerization and primary nucleation (see Section 1.4), but further studies would be needed to confirm this with full confidence. Repeating the SPR experiments in this study with immobilized αS oligomers and additional replicates with monomers could therefore prove very useful in further determination of binding affinities.

5.4 IMPLICATIONS FOR PARKINSON'S DISEASE

The accumulation and aggregation of αS are now considered integral parts of the mechanisms underlying PD[6]. Results from this study suggest 14-3-3η as a negative modulator of αS fibril onset and growth, which implicates an interesting role for this protein in PD pathology. Even in sub-stochiometric amounts of 10:1 and 2:1, 14-3-3η can decrease the αS fibrillation growth rate and possibly attenuate fibrillation onset *in vitro*, suggesting 14-3-3η as a possible neuroprotective factor in PD. While more extensive studies would be needed to validate this assumption, the study by Plotegher *et al*[9] demonstrated a complete suppression of αS fibrillation in αS:14-3-3η ratios of 4:1 and reduced αS-induced toxicity by overexpressing 14-3-3η, whereas the results in this study only demonstrated a delay in the fibrillation.

Moreover, *in vivo* studies demonstrated an upregulation of 14-3-3η transcription in aging mice overexpressing αS[65], indicating it may be part of a protective response to abnormal αS aggregation. Evidence that αS in overwhelming amounts could sequester 14-3-3η and thus cease its attenuating effects has also been suggested as a possible toxicity mechanism for αS oligomers[9]. Such sequestration could lead to the dysregulation of proteins normally regulated by 14-3-3η, and possibly other isoforms, thus depriving the cells of important regulatory functions. 14-3-3η is a suppressor of Parkin activity (see Section 1.7.2), a protein whose dysregulation is associated with PD[52]. Moreover, several 14-3-3 proteins, including 14-3-3η, have been discovered to bind and activate Tyrosine hydroxylase, a crucial enzyme in the biosynthesis of catecholamines like dopamine[66,67,46]. Hence, sequestration of 14-3-3η and possibly other isoforms could cause an un-timely activation of Parkin, and impairment of dopamine synthesis in PD. Interestingly, studies by Xu *et al*[11] suggested that αS accumulation induces neuronal apoptosis mediated by endogenous dopamine in dopaminergic cell lines, creating a paradox as to whether impaired dopamine synthesis could actually be beneficial to the already damaged cells. However, they further observed that elevated levels of αS/14-3-3 complexes increased neuronal vulnerability. 14-3-3s normally inactivate pro-apoptotic proteins like mitochondrial BAD and the Forkhead transcription factor. The sequestration into αS/14-3-3 complexes could thus reduce anti-apoptotic activity and make the dopaminergic neurons more vulnerable to reactive oxygen species generated by dopamine metabolism[11].

Altogether, observations in the literature as well as our own results could explain how overexpression of 14-3-3η reduces αS-induced toxicity[47], and thus why it is upregulated as a response to αS overexpression. Contradictory to these findings and the results of this study, *in vivo* experiments by Yacoubian et al[8] found 14-3-3η to be amongst 14-3-3 isoforms which did not affect αS aggregation nor reduce neurotoxicity. Further research on 14-3-3η is therefore required to uncover its exact role in PD pathology. Regardless, 14-3-3η appears to be intricately involved in the interplay of factors contributing to the overall pathogenesis and development of PD.

5.5 CONCLUSIONS

In this study, we aimed to investigate the influence of 14-3-3η on the kinetics of αS aggregation, and characterize the binding of 14-3-3η to αS. Our findings show 14-3-3η to decrease αS fibril growth rate by more than 50% in ratios of 10:1 and 2:1 (αS:14-3-3η). Although 14-3-3η did not induce significant changes in lag times, this can be attributed to the insufficient number of replicates and large variations resulting from the stochastic nature of fibrillation onset. Moreover, 14-3-3η yielded several flattened ThT fluorescence curves indicative of no αS fibrillation, not included in the statistical analysis. 14-3-3η also decreased the APPW over time, supporting that its influence on αS aggregation affects both fibrillation onset and growth *in vitro*. However, SPR experiments detected no interaction between 14-3-3η and monomeric αS, suggesting that it must interact with oligomeric species formed before fibrillation occurs. Despite that only one SPR replicate was obtained, this result is supported by NMR results from Plotegher *et al*[9]. The exact nature of this interaction remains unknown and merits further exploration. Regardless of mechanism, αS–14-3-3η interaction could provide an explanation for the 14-3-3η upregulation observed *in vivo* for mice overexpressing αS. Sequestration of 14-3-3η into αS fibrils also provides a possible toxicity mechanism for αS oligomers in PD.

To summarize, we found that 14-3-3η significantly attenuates the overall αS fibrillation process. We propose that 14-3-3η attenuates αS fibrillation rates and probably interferes with fibrillation onset through interaction with αS oligomeric species. We further conclude that a satisfactory fingerprint spectrum of 14-3-3η can be obtained through ^{2}H^{13}C^{15}N triple-labeling and ^{1}H^{15}N TROSY-HSQC, enabling for future binding site analysis. Lastly, we believe 14-3-

3η could emerge as a biomarker or even a therapeutic target in PD based on its connection to αS aggregation, providing a biomedical motivation for more extensive studies of this chaperone-like protein.

5.6 FUTURE PERSPECTIVES

The 14-3-3 family of proteins have been implicated in several human diseases, including PD[38]. Several isoforms have been detected in LBs from parkinsonian brains[47], and some isoforms are found to have neuroprotective effects both *in vitro* and *in vivo*[8]. The 14-3-3η isoform is one of the only isoforms demonstrated to directly influence the αS aggregation process[9]. This study thus focused on uncovering the direct effects of 14-3-3η on αS aggregation kinetics, and explore the interaction between 14-3-3η and αS. Although our findings indicate an attenuating role for 14-3-3η, further research is needed to fully understand how this isoform could be involved in αS aggregation and the pathological mechanisms in PD.

To gain a better understanding of 14-3-3η and its role in αS aggregation, it would be beneficial to repeat the *in vitro* aggregation assays of this study, acquiring a sufficient number of replicates to provide more statistical rigor. Implementing a wider range of 14-3-3η concentrations and longer experiment running times could provide new insights into critical αS:14-3-3η ratios for suppression of fibrillation. Furthermore, conducting aggregation assays with the remaining 14-3-3 isoforms would be an interesting approach to uncover whether the observed effects are isoform-specific to 14-3-3η. Moreover, studies of 14-3-3ζ have suggested that the capacity of its chaperone activity is greatly increased by the monomer configuration[44,45]. Hence, repeating the aggregation assays with monomeric 14-3-3η, e.g. by removing the dimerization site, could be an interesting approach to study how monomeric 14-3-3η compares to the dimer configuration with regards to αS aggregation. Additionally, the association of αS with lipids have been shown to greatly influence its aggregation propensity[26,27], demonstrated in this study by the strikingly different effects of BSA and FA-free BSA on αS fibrillation. Hence, it could be useful to repeat the experiments using lipids in the samples to investigate whether lipid association could affect the attenuation by 14-3-3η on αS aggregation.

Previous attempts have been made by Sato *et al*[52] and Plotegher *et al*[9] to determine how, and with what affinity, 14-3-3η binds αS. In this study, we attempted to utilize SPR and NMR to

uncover the properties of the interaction, however, time restrictions prevented the completion of these experiments. Proceeding with SPR experiments on 14-3-3η and αS monomers/oligomers could be the next step in determining binding affinities. Moreover, an interesting way to locate the 14-3-3η binding site would be to complete a backbone assignment using the triple-labeling and NMR scans described in this study, as well as aquiring triple-resonance experiments. Acquiring scans of 14-3-3η in the absence and presence of monomeric/oligomeric αS could then be used to detect the residues displaying the greatest chemical shift perturbations or reduction in signal intensities/peak volume, and thus are likely part of the binding site. Lastly, it would be interesting to repeat both aggregation and interaction experiments with αS phosphorylated at S129. Not only are the majority of 14-3-3 target proteins phosphorylated, but αS phosphorylation at S129 is the most prominent PTM observed in LBs and associated with αS aggregation[29]. Performing these experiments with phosphorylated αS would therefore elucidate upon the role of this PTM in the interaction between 14-3-3η and αS.

6. REFERENCES

1.   Soto, C. Unfolding the role of protein misfolding in neurodegenerative diseases. *Nat. Rev. Neurosci.* **4**, 49–60 (2003).

2.   Katsnelson, A., De Strooper, B. & Zoghbi, H. Y. Neurodegeneration: From cellular concepts to clinical applications. *Sci. Transl. Med.* **8**, 1–6 (2016).

3.   Ross, C. A. & Poirier, M. A. Protein aggregation and neurodegenerative disease. *Nat. Med.* **10**, S10 (2004).

4.   Kurtishi, A., Rosen, B., Patil, K. S., Alves, G. W. & Møller, S. G. Cellular Proteostasis in Neurodegeneration. *Mol. Neurobiol.* **56**, 3676–3689 (2019).

5.   Bourdenx, M. *et al.* Protein aggregation and neurodegeneration in prototypical neurodegenerative diseases: Examples of amyloidopathies, tauopathies and synucleinopathies. *Prog. Neurobiol.* **155**, 171–193 (2017).

6.   Xu, L. & Pu, J. Alpha-Synuclein in Parkinson ' s Disease : From Pathogenetic Dysfunction to Potential Clinical Application. **2016**, 1–10 (2016).

7.   Melo, T. Q., Copray, S. J. C. V. M. & Ferrari, M. F. R. Alpha-Synuclein Toxicity on Protein Quality Control, Mitochondria and Endoplasmic Reticulum. *Neurochem. Res.* **43**, 2212–2223 (2018).

8.   Yacoubian, T. A. *et al.* Differential neuroprotective effects of 14-3-3 proteins in models of Parkinson's disease. *Cell Death Dis.* **1**, 1–13 (2010).

9.   Plotegher, N. *et al.* The chaperone-like protein 14-3-3h interacts with human a-synuclein aggregation intermediates rerouting the amyloidogenic pathway and reducing a-synuclein cellular toxicity. *Hum. Mol. Genet.* (2014) doi:10.1093/hmg/ddu275.

10.   Logan, T., Bendor, J., Toupin, C., Thorn, K. & Edwards, R. H. α-Synuclein promotes dilation of the exocytotic fusion pore. *Nat. Neurosci.* (2017) doi:10.1038/nn.4529.

11.   Xu, J. *et al.* Dopamine-dependent neurotoxicity of α-synuclein: A mechanism for selective neurodegeneration in Parkinson disease. *Nat. Med.* **8**, 600–606 (2002).

12.   Galvagnion, C. The Role of Lipids Interacting with α-Synuclein in the Pathogenesis of Parkinson's Disease. *Journal of Parkinson's Disease* (2017) doi:10.3233/JPD-171103.

13.   Miraglia, F., Ricci, A., Rota, L. & Colla, E. Subcellular localization of alpha-synuclein aggregates and their interaction with membranes. *Neural Regen. Res.* **13**, 1136–1144 (2018).

14.   Chandra, S. *et al.* Double-knockout mice for α- and β-synucleins: Effect on synaptic functions. *Proc. Natl. Acad. Sci. U. S. A.* **101**, 14966–14971 (2004).

15.   Burré, J. The synaptic function of α-synuclein. *J. Parkinsons. Dis.* **5**, 699–713 (2015).

16.   Viennet, T. *et al.* Structural insights from lipid-bilayer nanodiscs link α-Synuclein membrane-binding modes to amyloid fibril formation. *Commun. Biol.* (2018) doi:10.1038/s42003-018-0049-z.

17. Cremades, N. *et al.* Direct observation of the interconversion of normal and toxic forms of α-synuclein. *Cell* **149**, 1048–1059 (2012).

18. Tuttle, M. D. *et al.* Solid-state NMR structure of a pathogenic fibril of full-length human α-synuclein. *Nat. Struct. Mol. Biol.* **23**, 409–415 (2016).

19. Jarrett, J. T. & Lansbury, P. T. Amyloid Fibril Formation Requires a Chemically Discriminating Nucleation Event: Studies of an Amyloidogenic Sequence from the Bacterial Protein OsmB. *Biochemistry* **31**, 12345–12352 (1992).

20. Buell, A. K. *et al.* Solution conditions determine the relative importance of nucleation and growth processes in α-synuclein aggregation. *Proc. Natl. Acad. Sci. U. S. A.* **111**, 7671–7676 (2014).

21. Luk, K. C. *et al.* Pathological a-Synuclein Transmission Initiates Parkinson-like Neurodegeneration in Nontransgenic Mice. *Science (80-.).* **338**, 949–954 (2012).

22. Winner, B. *et al.* In vivo demonstration that α-synuclein oligomers are toxic. *Proc. Natl. Acad. Sci. U. S. A.* **108**, 4194–4199 (2011).

23. Tokuda, T. *et al.* Detection of elevated levels of α-synuclein oligomers in CSF from patients with Parkinson disease. *Neurology* **75**, 1766–1772 (2010).

24. Wang, W., Nema, S. & Teagarden, D. Protein aggregation-Pathways and influencing factors. *Int. J. Pharm.* **390**, 89–99 (2010).

25. Suzuki, M., Sango, K., Wada, K. & Nagai, Y. Pathological role of lipid interaction with α-synuclein in Parkinson's disease. *Neurochem. Int.* **119**, 97–106 (2018).

26. Galvagnion, C. *et al.* Lipid vesicles trigger α-synuclein aggregation by stimulating primary nucleation. *Nat. Chem. Biol.* **11**, 229–234 (2015).

27. Zhu, M. & Fink, A. L. Lipid binding inhibits α-synuclein fibril formation. *J. Biol. Chem.* **278**, 16873–16877 (2003).

28. Galvagnion, C. *et al.* Chemical properties of lipids strongly affect the kinetics of the membrane-induced aggregation of α-synuclein. *Proc. Natl. Acad. Sci. U. S. A.* **113**, 7065–7070 (2016).

29. Pajarillo, E., Rizor, A., Lee, J., Aschner, M. & Lee, E. The role of posttranslational modifications of α-synuclein and LRRK2 in Parkinson's disease: Potential contributions of environmental factors. *Biochim. Biophys. Acta - Mol. Basis Dis.* 0–1 (2018) doi:10.1016/j.bbadis.2018.11.017.

30. Lee, K. W. *et al.* Enhanced phosphatase activity attenuates α-synucleinopathy in a mouse model. *J. Neurosci.* **31**, 6963–6971 (2011).

31. Krumova, P. *et al.* Sumoylation inhibits α-synuclein aggregation and toxicity. *J. Cell Biol.* **194**, 49–60 (2011).

32. Klaips, C. L., Jayaraj, G. G. & Hartl, F. U. Pathways of cellular proteostasis in aging and disease. *J. Cell Biol.* **217**, 51–63 (2018).

33. Bandopadhyay, R. & de Belleroche, J. Pathogenesis of Parkinson's disease: emerging role of molecular chaperones. *Trends Mol. Med.* **16**, 27–36 (2010).

34. Dedmon, M. M., Christodoulou, J., Wilson, M. R. & Dobson, C. M. Heat shock protein 70 inhibits α-synuclein fibril formation via preferential binding to prefibrillar species. *J. Biol. Chem.* **280**, 14733–14740 (2005).

35. Shendelman, S., Jonason, A., Martinat, C., Leete, T. & Abeliovich, A. DJ-1 Is a redox-dependent molecular chaperone that inhibits α-synuclein aggregate formation. *PLoS Biol.* **2**, (2004).

36. Yaffe, M. B. *et al.* The Structural Basis for 14-3-3 : Phosphopeptide Binding Specificity. *Cell* **91**, 961–971 (1997).

37. Aitken, A. 14-3-3 proteins: A historic overview. *Semin. Cancer Biol.* **16**, 162–172 (2006).

38. Cau, Y., Valensin, D., Mori, M., Draghi, S. & Botta, M. Structure, Function, Involvement in Diseases and Targeting of 14-3-3 Proteins: An Update. *Curr. Med. Chem.* **25**, 5–21 (2017).

39. Xu, Z. *et al.* 14-3-3 Protein Targets Misfolded Chaperone-Associated Proteins To Aggresomes. *J. Cell Sci.* **126**, 4173–4186 (2013).

40. Rittinger, K. *et al.* Structural analysis of 14-3-3 phosphopeptide complexes identifies a dual role for the nuclear export signal of 14-3-3 in ligand binding. *Mol. Cell* **4**, 153–166 (1999).

41. Sluchanko, N. N. & Gusev, N. B. Moonlighting chaperone-like activity of the universal regulatory 14-3-3 proteins. *FEBS J.* **284**, 1279–1295 (2017).

42. Silhan, J. *et al.* 14-3-3 Protein C-terminal stretch occupies ligand binding groove and is displaced by phosphopeptide binding. *J. Biol. Chem.* **279**, 49113–49119 (2004).

43. Coblitz, B., Wu, M., Shikano, S. & Li, M. C-terminal binding: An expanded repertoire and function of 14-3-3 proteins. *FEBS Lett.* **580**, 1531–1535 (2006).

44. Woodcock, J. M. *et al.* Role of salt bridges in the dimer interface of 14-3-3ζ in dimer dynamics, N-terminal α-helical order, and molecular chaperone activity. *J. Biol. Chem.* **293**, 89–99 (2018).

45. Sluchanko, N. N. & Gusev, N. B. Oligomeric structure of 14-3-3 protein: What do we know about monomers? *FEBS Lett.* **586**, 4249–4256 (2012).

46. Steinacker, P., Aitken, A. & Otto, M. 14-3-3 Proteins in Neurodegeneration. *Semin. Cell Dev. Biol.* **22**, 696–704 (2011).

47. Fan, X. *et al.* 14-3-3 Proteins Are on the Crossroads of Cancer, Aging, and Age-Related Neurodegenerative Disease. *Int. J. Mol. Sci.* **20**, (2019).

48. Wiltfang, J. *et al.* Isoform pattern of 14-3-3 proteins in the cerebrospinal fluid of patients with Creutzfeldt-Jakob disease. *J. Neurochem.* **73**, 2485–2490 (1999).

49. Berg, D., Riess, O. & Bornemann, A. Specification of 14-3-3 proteins in Lewy bodies [1]. *Ann. Neurol.* **54**, 135 (2003).

50. UniProtKB. Q04917 (1433F_HUMAN). https://www.uniprot.org/uniprot/Q04917.

51. Ubl, A. *et al.* 14-3-3 protein is a component of Lewy bodies in Parkinson's disease - Mutation analysis and association studies of 14-3-3 eta. *Mol. Brain Res.* **108**, 33–39 (2002).

52. Sato, S. *et al.* 14-3-3H Is a Novel Regulator of Parkin Ubiquitin Ligase. *EMBO J.* **25**, 211–221 (2006).

53. Kitada, T. *et al.* Mutations in the parkin gene cause autosomal recessive juvenile parkinsonism. *Nat. Lett.* **169**, 166–169 (1998).

54. Wördehoff, M. & Hoyer, W. α-Synuclein Aggregation Monitored by Thioflavin T Fluorescence Assay. *Bio-Protocol* **8**, (2018).

55. Xue, C., Lin, T. Y., Chang, D. & Guo, Z. Thioflavin T as an amyloid dye: Fibril quantification, optimal concentration and effect on aggregation. *R. Soc. Open Sci.* **4**, (2017).

56. Lesk M, A. *Introduction to Protein Science: Architecture, function and genomics*. (Oxford University Press, 2016).

57. Arrowsmith, C. H. & Yu-Sung, W. NMR of large (s> 25 kDa) proteins and protein complexes. *Prog. Nucl. Magn. Reson. Spectrosc.* **32**, 277–286 (1998).

58. Pervushin, K., Riek, R., Wider, G. & Wüthrich, K. Attenuated T2 relaxation by mutual cancellation of dipole-dipole coupling and chemical shift anisotropy indicates an avenue to NMR structures of very large biological macromolecules in solution. *Proc. Natl. Acad. Sci. U. S. A.* **94**, 12366–12371 (1997).

59. Wilson, K. & Walker, J. *Principles and Techniques of Biochemistry and Molecular Biology*. (Cambridge University Press, 2018).

60. Lashuel, H. A., Overk, C. R., Oueslati, A. & Masliah, E. The many faces of α-synuclein: From structure and toxicity to therapeutic target. *Nat. Rev. Neurosci.* **14**, 38–48 (2013).

61. Bermel, W. *et al.* Protonless NMR experiments for sequence-specific assignment of backbone nuclei in unfolded proteins. *J. Am. Chem. Soc.* **128**, 3918–3919 (2006).

62. Marion, D. An introduction to biological NMR spectroscopy. *Mol. Cell. Proteomics* **12**, 3006–3025 (2013).

63. Cavanagh, J., Skelton, N., Fairbrother, W., Rance, M. & Palmer, A. *Protein NMR Spectroscopy*. (Academic Press, 2006).

64. Killoran, R. C., Fan, J., Yang, D., Shilton, B. H. & Choy, W. Y. Structural analysis of the 14-3-3ζ/Chibby interaction involved in Wnt/β-catenin signaling. *PLoS One* **10**, 1–19 (2015).

65. Brehm, N., Rau, K., Kurz, A., Gispert, S. & Auburger, G. Age-related changes of 14-3-3 isoforms in midbrain of A53T-SNCA overexpressing mice. *J. Parkinsons. Dis.* **5**, 595–604 (2015).

66. Ichimura, T. *et al.* Molecular cloning of cDNA coding for brain-specific 14-3-3 protein, a protein kinase-dependent activator of tyrosine and tryptophan hydroxylases. *Proc. Natl. Acad. Sci. U. S. A.* **85**, 7084–7088 (1988).

67. Halskau, Ø. *et al.* Three-way interaction between 14-3-3 proteins, the N-terminal region of

tyrosine hydroxylase, and negatively charged membranes. *J. Biol. Chem.* **284**, 32758–32769 (2009).

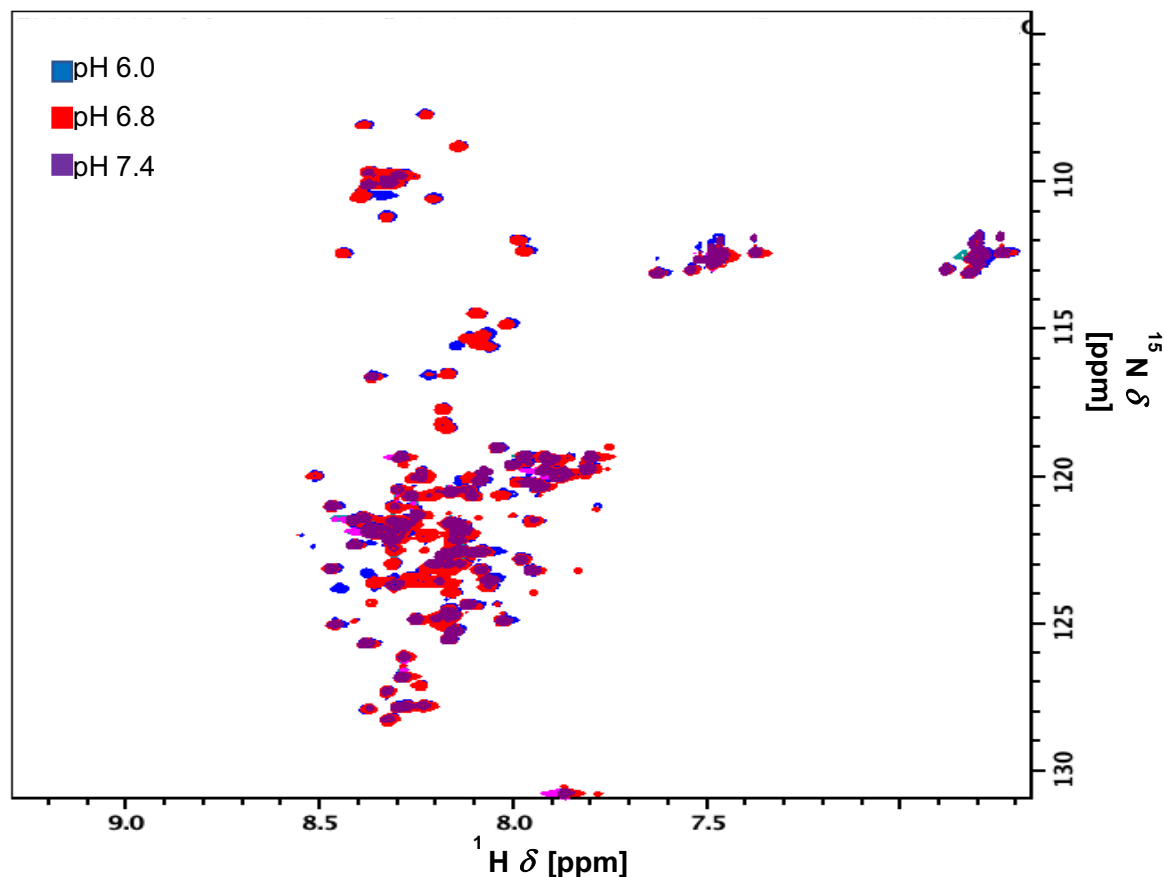# 7. SUPPLEMENTARY DATA

7.1 NMR SPECTROSCOPY

Figure 7.1 – Overlay of 2D HSQC spectra from ^{13}C ^{15}N-labeled αS in various pH conditions. The HSQC fingerprints of 180 μM $^{13}C^{15}N$-labeled αS at pH 6.0 (blue), 6.8 (red) and 7.4 (purple) were similar in their sensitivity and detection of cross-peaks. Closely dispersed peaks along the F2 (^{1}H chemical shift, δ) and F1 (^{15}N chemical shift, δ) axis are indicates of an unfolded protein, corresponding to the intrinsically disordered native state of αS. However, certain peaks were only detected in αS pH 6.0 – this pH value was thus used for further NMR experiments. Data were collected at 25°C on the 850 MHz Bruker Advanced III HD Spectrometer.
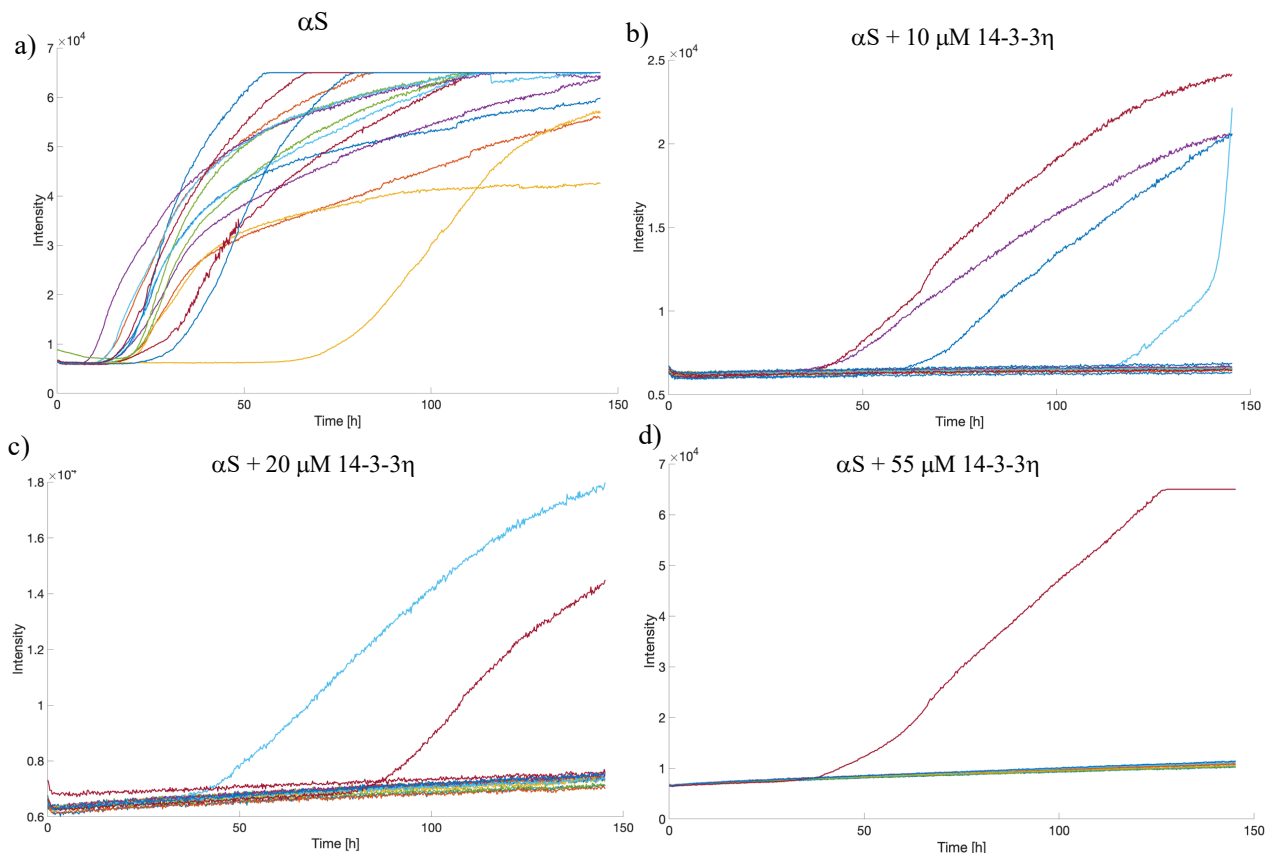
7.2 THT-MONITORED AGGREGATION ASSAYS

Figure 7.2 – ThT-monitored αS fibrillation curves in the absence and presence of 14-3-3η, 1st replicate. *The aggregation of αS was monitored by the fibril-dependent fluorescence of ThT, creating a fluorescent signal increasing with fibril growth. Samples were prepared with 100 μM αS and 5 μM ThT in each sample, and 10-55 μM of 14-3-3η, with 15 wells/sample. Data were collected with FLUOStar Optima Microplate Fluorescence Reader. The selection of fibrillation curves shows the development of ThT fluorescence and thus fibrillation in a) 100 μM αS, b) αS + 10 μM 14-3-3η, c) αS + 20 μM 14-3-3η, and d) αS + 55 μM 14-3-3η.*
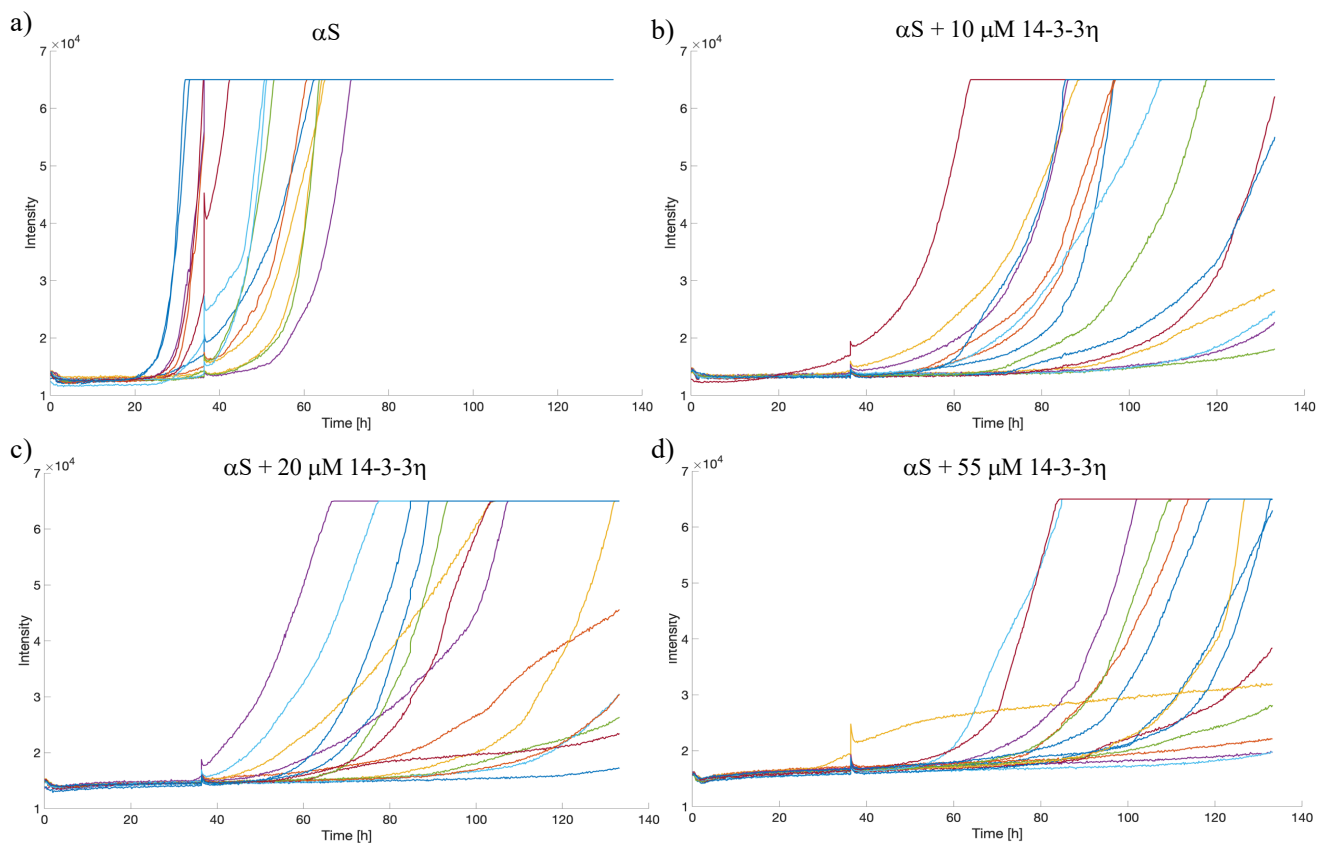
Figure 7.3 – ThT-monitored αS fibrillation curves in the absence and presence of 14-3-3η, 2ⁿᵈ replicate.
The aggregation of αS was monitored by the fibril-dependent fluorescence of ThT, creating a fluorescent signal increasing with fibril growth. Samples were prepared with 100 μM αS and 5 μM ThT in each sample, and 10-55 μM of 14-3-3η, with 15 wells/sample. Data were collected with FLUOStar Optima Microplate Fluorescence Reader. The selection of fibrillation curves shows the development of ThT fluorescence and thus fibrillation in a) 100 μM αS, b) αS + 10 μM 14-3-3η, c) αS + 20 μM 14-3-3η, and d) αS + 55 μM 14-3-3η.
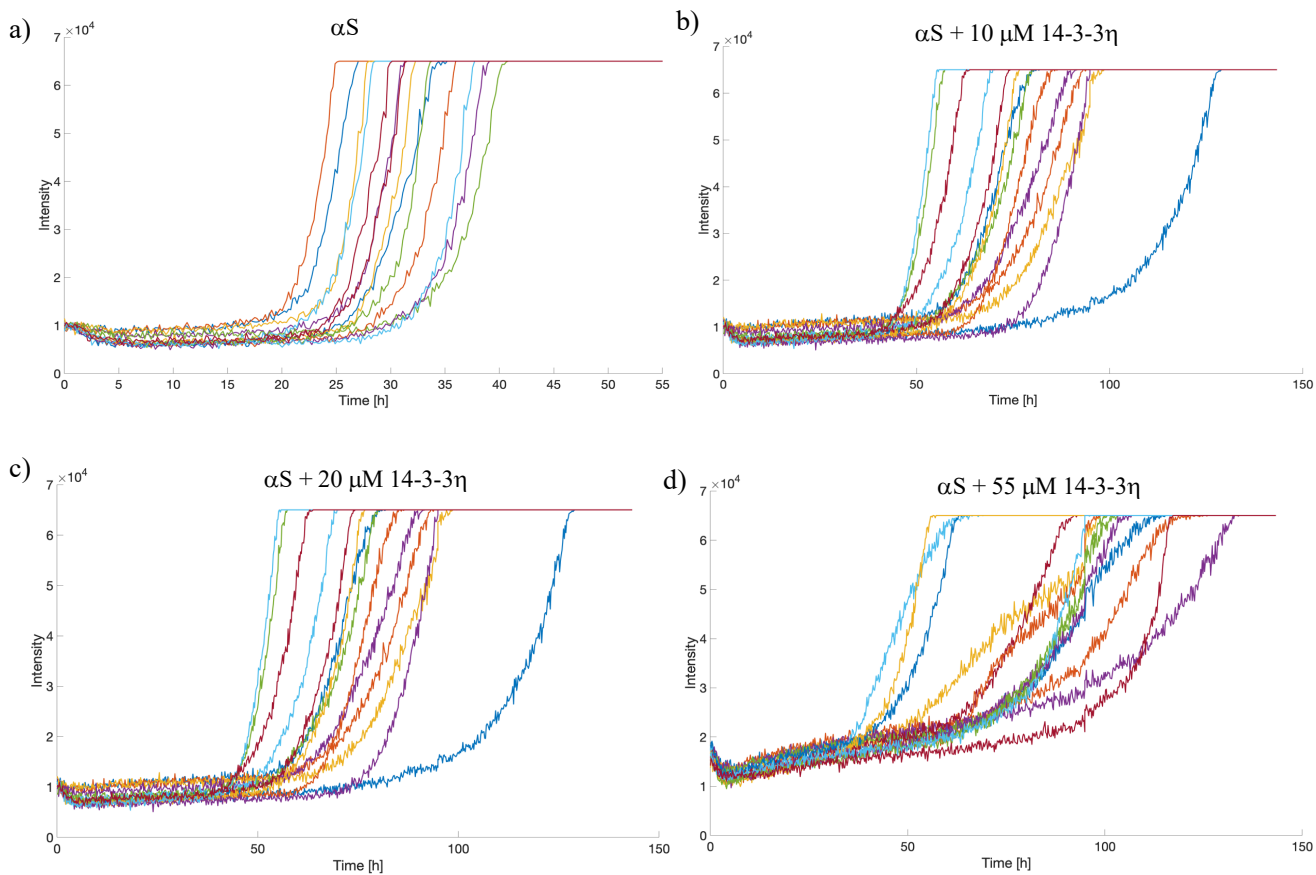
Figure 7.4 – ThT-monitored αS fibrillation curves in the absence and presence of 14-3-3η, 3rd replicate. The aggregation of αS was monitored by the fibril-dependent fluorescence of ThT, creating a fluorescent signal increasing with fibril growth. Samples were prepared with 100 μM αS and 5 μM ThT in each sample, and 10-55 μM of 14-3-3η, with 15 wells/sample. Data were collected with FLUOStar Optima Microplate Fluorescence Reader. The selection of fibrillation curves shows the development of ThT fluorescence and thus fibrillation in a) 100 μM αS, b) αS + 10 μM 14-3-3η, c) αS + 20 μM 14-3-3η, and d) αS + 55 μM 14-3-3η.
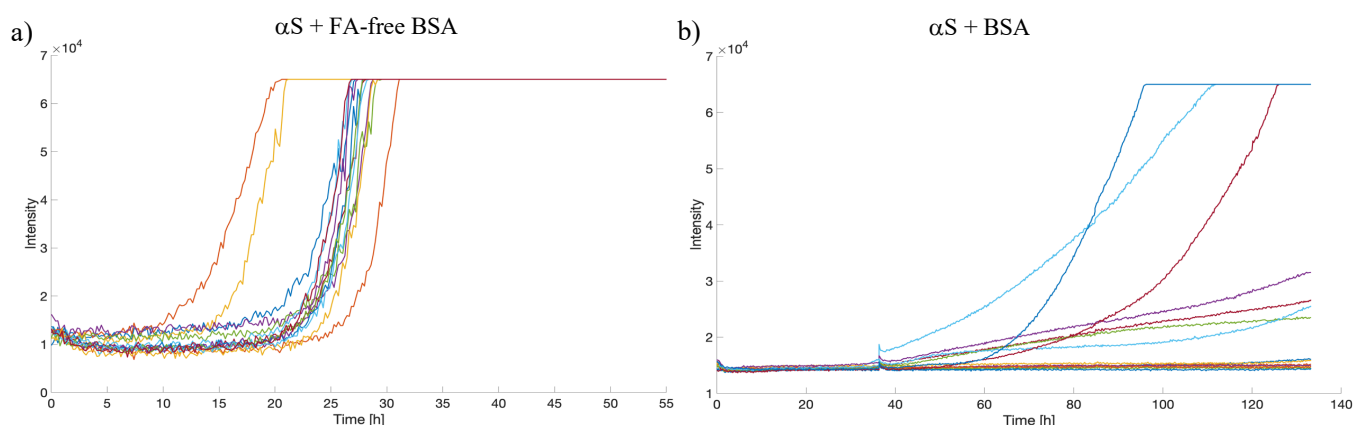
Figure 7.5 – ThT-monitored αS fibrillation curves in the presence of BSA and FA-free BSA protein controls. The aggregation of αS was monitored by the fibril-dependent fluorescence of ThT, creating a fluorescent signal increasing with fibril growth. Samples were prepared with 100 µM αS and 5 µM ThT in each sample and 15 wells/sample. Data were collected with FLUOStar Optima Microplate Fluorescence Reader. The fibrillation curves show fibrillation development of a) αS + 55 µM FA-free BSA, from the 3rd replicate, and b) αS + 55 µM BSA, from the 2nd replicate.

Table 7.1a: Mean fibrillation lag times (t_n) normalized to αS control

Sample	100 µM αS	αS + 55 µM BSA	αS + 55 µM FA-free BSA	αS + 10 µM 14-3-3η	αS + 20 µM 14-3-3η	αS + 55 µM 14-3-3η
t_n, 1st replicate (%)	100	-	-	279.7	337.7	139.5
t_n, 2nd replicate (%)	100	115.8	-	162.9	148.6	159.0
t_n, 3rd replicate (%)	100	-	81.0	220.4	232.9	199.6
Mean t_n (%)	**100**	**115.8**	**81.0**	**221.0**	**239.8**	**166.1**
Std. Dev	0	-	-	58.36	99.73	30.69

Table 7.1b: *P*-values from statistical analysis (Welch t-test) of mean fibrillation lag times (t_n), significance level $\alpha = 0.05$

	100µM αS	αS + 10µM 14-3-3η	αS + 20µM 14-3-3η	αS + 55µM 14-3-3η
100 µM αS	-			
αS + 10µM 14-3-3η	0.07	-		
αS + 20µM 14-3-3η	0.1	0.8	-	
αS + 55µM 14-3-3η	0.07	0.2	0.3	-

Table 7.2a: Mean fibrillation rates (ν) normalized to αS control

Sample	100 µM αS	αS + 55 µM BSA	αS + 55 µM FA-free BSA	αS + 10 µM 14-3-3η	αS + 20 µM 14-3-3η	αS + 55 µM 14-3-3η
ν, 1st replicate (%)	100	-	-	68.5	78.5	55.3
ν, 2nd replicate (%)	100	12.7	-	28.0	22.8	25.3
ν, 3rd replicate (%)	100	-	97.6	30.2	21.1	14.3
Mean ν (%)	**100**	**12.7**	**97.6**	**42.2**	**40.8**	**31.6**
Std. Dev	0	-	-	22.7	32.7	21.2

Table 7.2b: *P*-values from statistical analysis (Welch t-test) of mean fibrillation rates (ν), significance level $\alpha = 0.05$

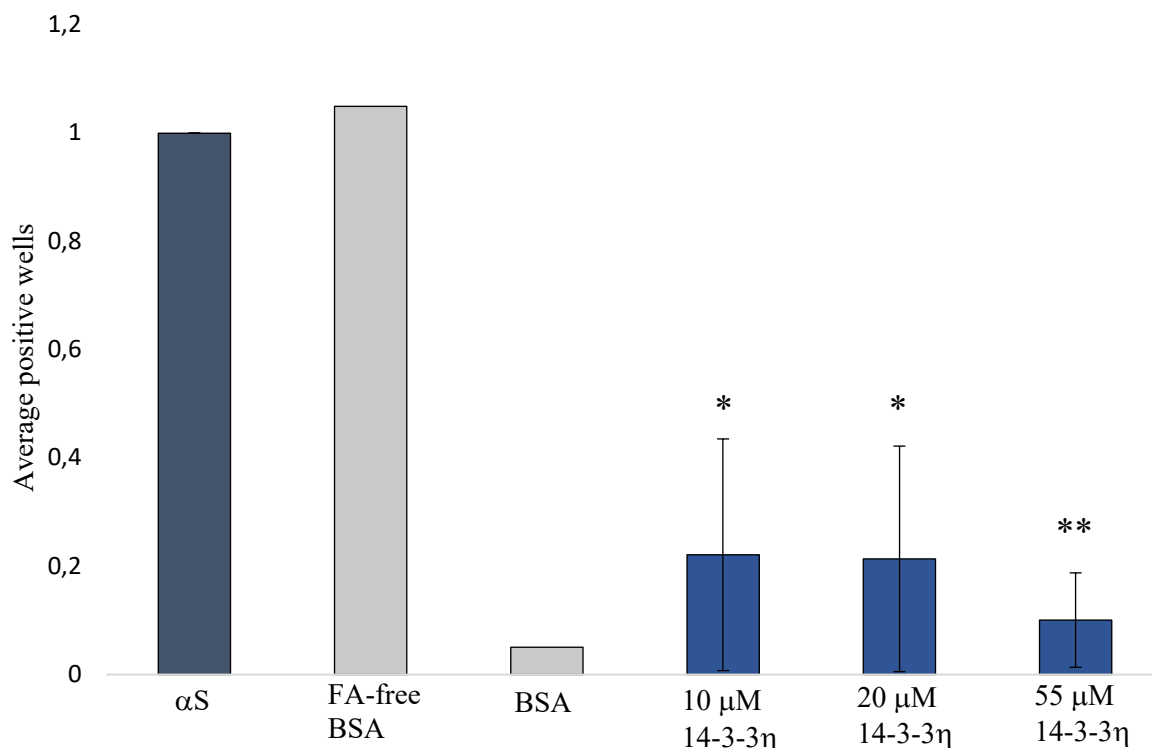|	100µM αS	αS + 10µM 14-3-3η	αS + 20µM 14-3-3η	αS + 55µM 14-3-3η
100 µM αS	-			
αS + 10µM 14-3-3η	**0.04***	-		
αS + 20µM 14-3-3η	0.08	0.9	-	
αS + 55µM 14-3-3η	**0.03***	0.6	0.7	-

Figure 7.6 – Average percentage of aggregation positive wells over 140 hr, normalized to αS control.
The aggregation of αS were monitored over time by the fibril-dependent fluorescence of ThT, creating a fluorescent signal increasing with fibril growth. A cumulative analysis was performed to find the percentage of aggregation positive wells/sample, i.e. where the fluorescent signal ascended three-fold of the noise. The average percentages over time for each sample were normalized to the αS control. 14-3-3η significantly (*) decreased the average percentage of positive wells.

Table 7.3: *P*-values from statistical analysis (Welch t-test) of the average percentage of aggregation positive wells, significance level α = 0.05

	100µM αS	αS + 10µM 14-3-3η	αS + 20µM 14-3-3η	αS + 55µM 14-3-3η
100 µM αS	-			
αS + 10µM 14-3-3η	**0.02***	-		
αS + 20µM 14-3-3η	**0.02***	0.9	-	
αS + 55µM 14-3-3η	**0.003****	0.5	0.5	-